

Beyond maps: Patterns of formation processes at the Middle Pleistocene open-air site of Marathousa 1, Megalopolis Basin, Greece

Domenico Giusti^{a,*}, Vangelis Tourloukis^a, George E. Konidaris^a,
Nicholas Thompson^a, Panagiotis Karkanas^b, Eleni Panagopoulou^c, Katerina Harvati^a

^a*Paläoanthropologie, Senckenberg Centre for Human Evolution and Palaeoenvironment, Eberhard Karls Universität Tübingen, Rümelinstr. 23, 72070 Tübingen, Germany*

^b*Malcolm H. Wiener Laboratory for Archaeological Science, American School of Classical Studies at Athens, Greece*

^c*Ephoreia of Palaeoanthropology-Speleology of Greece, Athens, Greece*

Abstract

Recent excavations at the Middle Pleistocene open-air site of Marathousa 1 have unearthed in one of the two investigated areas (Area A) a partial skeleton of a single individual of *Palaeoloxodon antiquus* and other faunal remains in spatial and stratigraphic association with lithic artefacts. In Area B, a much higher number of lithic artefacts was collected, spatially and stratigraphically associated also with faunal remains. The two areas are stratigraphically correlated, the main fossiliferous layers representing an *en masse* depositional process in a lake margin context. Evidence of butchering (cut-marks) has been identified on bones of the elephant skeleton, as well on elephant and other mammal bones from Area B. However, due to the secondary deposition of the main find-bearing units, it is of primary importance to evaluate the degree and reliability of the spatial association of the lithic artefacts with the faunal remains. Indeed, spatial association does not necessarily imply causation, since natural syn- and post-depositional processes may equally produce spatial association. Assessing the degree and extent of post-depositional reworking processes is crucial to fully comprehend the archaeological record, and therefore to reliably interpret past human behaviours. The present study uses a comprehensive set of spatial statistics in order to disentangle the depositional processes behind the distribution of the archaeological and palaeontological record at Marathousa 1. Preliminary results of our analyses suggest that a high-energy erosional process, attributed to a hyperconcentrated flow deposited at the margin of a swamp, reworked an autochthonous, exposed or slightly buried, scatter of lithic artefacts and faunal remains. Minor reworking and substantial spatial association of the lithic and faunal assemblages support the current interpretation of Marathousa 1 as a butchering site.

Keywords: Spatial analysis, Site formation processes, Vertical distribution, Fabric

*Corresponding author

Email address: domenico.giusti@uni-tuebingen.de (Domenico Giusti)

1. Introduction

2 Archaeological site formation processes, intensively studied since the early 1970s
3 (Isaac, 1967; Schiffer, 1972, 1983, 1987; Shackley, 1978; Wood and Johnson, 1978;
4 Binford, 1981; Schick, 1984, 1986, 1987; Petraglia and Nash, 1987; Petraglia and
5 Potts, 1994, among others), “still insufficiently taken in consideration” (Texier, 2000,
6 p.379) at the beginning of the 21st century, are nowadays fully acknowledged in the ar-
7 chaeological practice (Villa, 2004; Bailey, 2007; Brantingham et al., 2007; Malinsky-
8 Buller et al., 2011; Vaquero et al., 2012; Bargalló et al., 2016, among others). Drawing
9 inferences about past human behaviours from scatters of archaeological remains must
10 account for syn- and post-depositional contextual processes.

11 Several methods are currently applied in order to qualify and quantify the type and
12 degree of reworking of archaeological assemblages. Within the framework of a geoar-
13 chaeological and taphonomic approach, spatial statistics offer meaningful contributions
14 in unravelling site formation and modification processes from spatial patterns. How-
15 ever, while the spatio-temporal dimension is an ineluctable inherent property of any
16 biotic and abiotic process, spatial statistics are still insufficiently applied.

17 Distribution maps are cornerstones of the archaeological documentation process
18 and are primary analytic tools. However, their visual interpretation is prone to subjec-
19 tivity and is not reproducible (Bevan et al., 2013). Since the early 1970's (see Hodder
20 and Orton (1976); Orton (1982) and references therein), the traditional, intuitive, ‘eye-
21 balling’ method of spotting spatial patterns has been abandoned in favour of more ob-
22 jective approaches, extensively borrowed from other fields. Nevertheless, quantitative
23 methods, while still percolating in the archaeological sciences from neighbouring dis-
24 ciplines, are not extensively used. Moreover, only a relatively small number of studies
25 have explicitly applied spatial point pattern analysis or geostatistics to the study of site
26 formation and modification processes (Lenoble et al., 2008; Domínguez-Rodrigo et al.,
27 2014b,a, 2017; Carrer, 2015; Giusti and Arzarello, 2016; Organista et al., 2017, but see
28 Hivernel and Hodder (1984) for an earlier work on the subject).

29 The goal of a taphonomic approach to spatial analysis is to move beyond distri-
30 bution maps by applying a comprehensive set of multiscale and multivariate spatial
31 statistics in order to reliably construct inferences from spatial patterns. An exhaustive
32 spatial analytic approach to archaeological inference, combined with a taphonomic
33 perspective, is essential for evaluating the depositional processes and integrity of the
34 archaeological assemblage, and consequently for a reliable interpretation of past hu-
35 man behaviours.

36 The present study uses a comprehensive set of spatial statistics in order to disentan-
37 gle the depositional processes behind the spatial distribution of the archaeological and
38 palaeontological record recovered during excavation at the Middle Pleistocene open-air
39 site of Marathousa 1, Megalopolis, Greece (Panagopoulou et al., 2015; Harvati et al.,
40 2016).

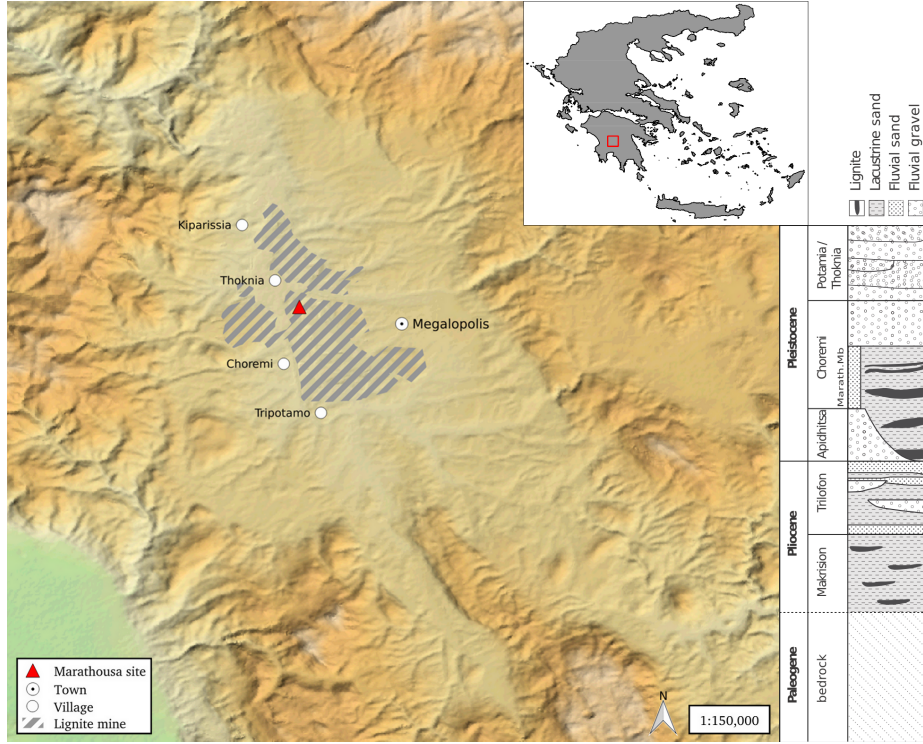


Figure 1: Geographical location of the Marathousa 1 site in the Megalopolis basin and stratigraphic column of the basin, modified after [van Vugt et al. \(2000\)](#).

41 1.1. Marathousa 1

42 The site (Fig. 1), discovered in 2013 at the edge of an active lignite quarry, is
 43 located between two lignite seams in the Pleistocene deposits of the Megalopolis basin,
 44 Marathousa Member of the Choremi Formation ([van Vugt et al., 2000](#)). The regular
 45 alternation of lacustrine clay, silt and sand beds with lignite seams has been interpreted
 46 having cyclic glacial (or stadial) and interglacial (or interstadial) origin ([Nickel et al.,
 47 1996](#)). The half-graben configuration of the basin, with major subsidence along the
 48 NW-SE trending normal faults along the eastern margin, resulted in the gentle dip of
 49 the lake bottom at the opposite, western, margin of the lake, enabling the formation of
 50 swamps and the accumulation of organic material for prolonged periods of time ([van
 51 Vugt et al., 2000](#)).

52 Two excavation areas have been investigated since 2013 (Fig. 2): Area A, where
 53 several skeletal elements of a single individual of *Palaeoloxodon antiquus* have been
 54 unearthed, together with a number of lithic artefacts and other faunal remains; and
 55 Area B, located 60 m to the South along the exposed section, where the lithic assem-
 56 blage is richer and occurs in association with a faunal assemblage composed of isolated
 57 elephant bones, cervids and carnivores among others. Bones from Area B are charac-
 58 terized by a high degree of fragmentation (bone fragments make up 93.4% of the as-

59 semblage), with their maximal diameter mostly measuring less than 80mm ([Konidaris](#)
60 [et al., this issue](#); [Tourloukis et al., this issue](#)). Evidence of butchering (cut-marks) have
61 been identified on two of the elephant bones from Area A, as well on elephant and
62 other mammal bones from Area B ([Konidaris et al., this issue](#)).

63 The sedimentary sequence of the site (Fig. 3) includes lacustrine and fluvio-lacustrine
64 clastic deposits sandwiched between two lignite seams (UA7-UB10 and UA1-UB1)
65 ([Karkanas et al., this issue](#)). A major hiatus (contacts between UA3 and UA4, and
66 between UB5 and UB6), attributed to exposure and erosion of a lake shore mudflat,
67 divides the sequence in two parts. The lower part is characterised by relatively high
68 rate sub-aqueous sedimentation of bedded sands and silts, containing low organic and
69 carbonate content. The upper one is characterised by a series of erosional bounded
70 depositional units, attributed to sub-aerial originated organic- and carbonate-rich mud
71 flows and hyperconcentrated flows deposited at the margin of a swamp ([Karkanas et al.,](#)
72 [this issue](#)).

73 The erosional contacts UA3c/4 and UB4c/5a separate the two main find-bearing
74 units in both areas (Fig. 3). In Area A, the elephant remains lie at the contact of UA3c/4
75 and are covered by UA3c (Fig. 4a); while in Area B, most of the remains were collected
76 from unit UB4c (Figs. 2 and 4b). Units UA3c and UB4c (organic- and intraclast-rich
77 silty sands) resemble dilute mud flows, showing a chaotic structure of rip-up clasts
78 from the underlying unit, small-to-large wood fragments and rare rock clasts. In Area
79 B, a relatively low number of remains was also found in massive organic-rich silty
80 sands (UB5a, Fig. 2), which locally overlay channelised sands (UB5b/c), probably not
81 preserved in Area A ([Karkanas et al., this issue](#)).

82 The flow event described above (units UA3c and UB4c), and specifically the ero-
83 sional contacts between the fossiliferous horizons in the two areas (UA3c/4 and UB4c/5a),
84 provide the essential background for the analysis and interpretation of the spatial distri-
85 butions at Marathousa 1. The secondary depositional nature of the main find horizons
86 raises the question of how reliable is the spatial association between the lithic arte-
87 facts and the partial skeleton of a single *Palaeoloxodon antiquus* individual and other
88 faunal remains. Since spatial association does not necessarily imply causation, and
89 consequently synchrony, the answer has important consequences for the interpretation
90 of the site in the broader context of the Middle Pleistocene human-proboscidean inter-
91 actions. We aim to tackle this question and disentangle the formation processes acting
92 at Marathousa 1 on the basis of spatial patterns through a three-prong spatial analytic
93 approach:

- 94 1. By analysing, in a frame of references, the orientation patterns of remains from
95 relevant stratigraphic units;
- 96 2. By quantifying and comparing their relative vertical distributions;
- 97 3. By identifying spatial trends in either the assemblage intensities and the associa-
98 tions between classes of remains.

99 Two contrasting models of deposition are tested: the autochthonous hypothesis
100 (*sensu* [Fernández-López, 1991](#); [Domínguez-Rodrigo et al., 2012](#)) states that the flow
101 event, represented by units UA3c and UB4c, eroded and scoured the exposed surface
102 (where the elephant was lying), thereby entraining clastic material (including arte-
103 facts) and re-depositing (*sensu* [Fernández-López, 1991](#)) this material at a close dis-

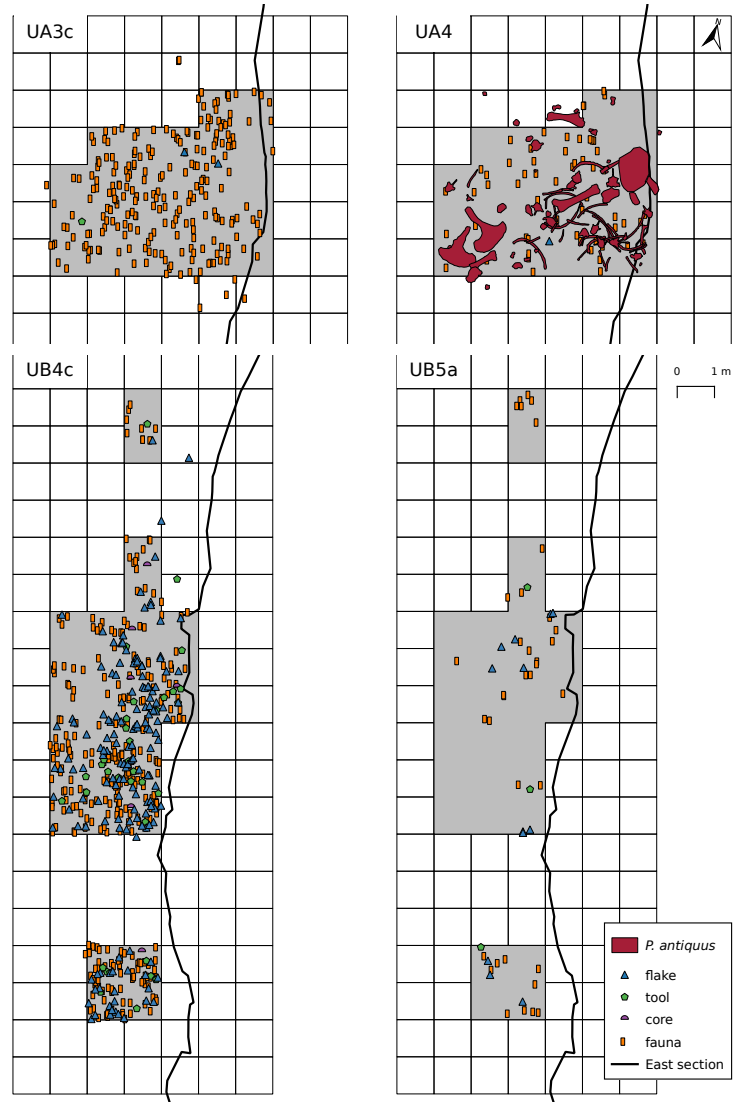


Figure 2: Distribution maps of the plotted remains from areas A (units UA3c and UA4) and B (units UB4c and UB5a), collected until 2015. Due to their high number, lithic debris/chips are not plotted. The plotted remains of the *P. antiquus* skeleton were collected until 2016. Grey zones mark the 2013-2015 excavation areas. Area B is located 60 m to the South, along the exposed East section of the lignite quarry.

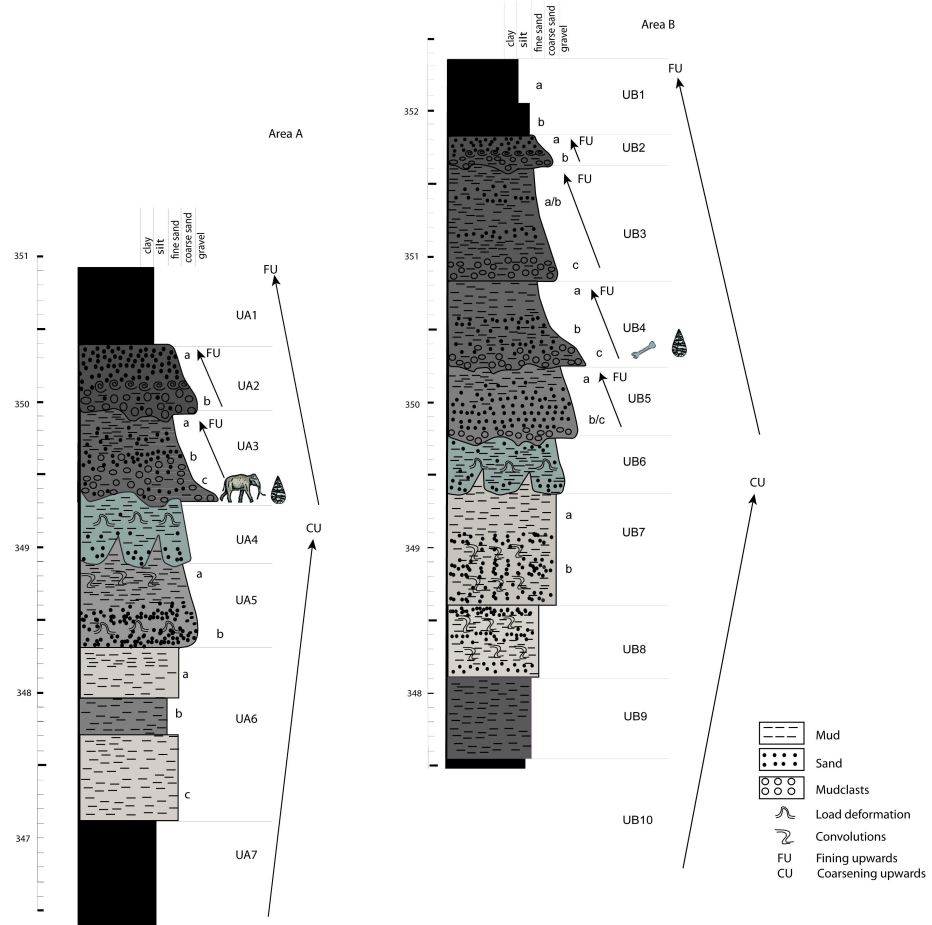


Figure 3: Stratigraphic setting of the Marathousa 1 site, modified after Karkanas et al. ([this issue](#)). Absolute elevations in m a.s.l.

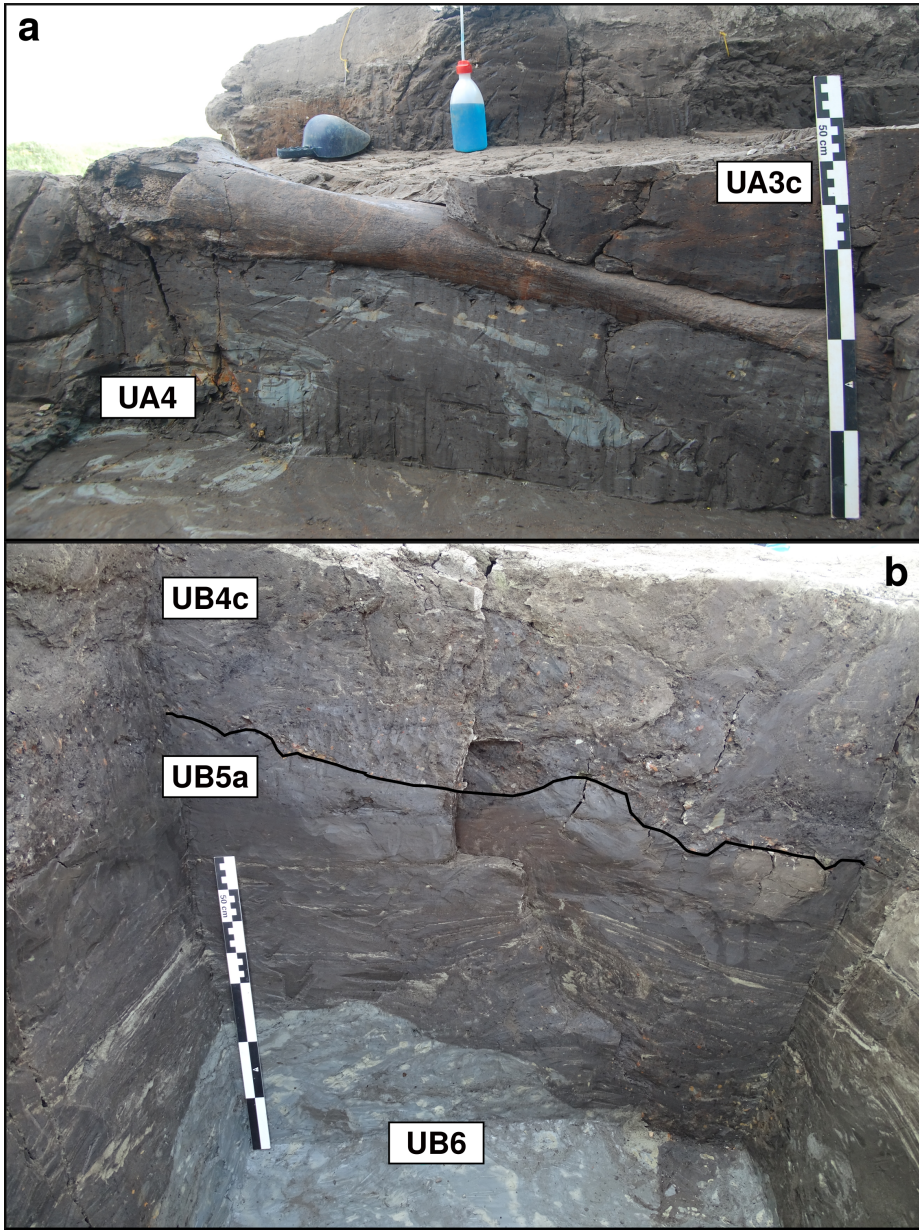


Figure 4: Photograph (2017) of the left femur of the *P. antiquus* skeleton, lying at the UA3c/4 contact and covered by unit UA3c (a). West profile (2014) of the excavation Area B (square 932/603), exposing the UB4c/5a (black solid line) and the UB5/6 erosional contacts (b).

104 tance. This model implies the loss of any original, pristine spatial relations between
105 remains, but minor transport from the primary depositional *loci*. On the other hand, the
106 allochthonous hypothesis (*sensu* Fernández-López, 1991; Domínguez-Rodrigo et al.,
107 2012) implies significant transport from the original *loci* of deposition and re-elaboration
108 (*sensu* Fernández-López, 1991). According to this model, the spurious spatial associa-
109 tion between the lithic artefacts and faunal remains does not support any behavioural
110 interpretation.

111 2. Material and methods

112 Since 2013, systematic investigation of the Marathousa 1 site has been carried out
113 by a joint team from the Ephoreia of Palaeoanthropology-Speleology (Greek Ministry
114 of Culture) and the University of Tübingen. A grid system of 1 square meter units
115 was set up, oriented -14 degrees off the magnetic North, and including the two areas
116 of investigation. The excavation of the deposit proceeded in 50x50 cm sub-squares in
117 Area B and 1x1 m squares in Area A, and spits of 5 to 10 cm thickness, respectively.
118 Systematic water-screening of sediments was carried out on-site using 1 mm sieves
119 in order to guarantee recovery of the small-size fraction (e.g., micro-artefacts, small
120 mammal remains, fish, molluscs and small fragments of organic and inorganic mate-
121 rial). The three-dimensional coordinates of finds (i.e., all the lithic artefacts, teeth and
122 diagnostic bones; bones and organic material with a-axis ≥ 20 mm), collected spits
123 of sediment, samples and geological features (e.g., erosional contacts and mud cracks)
124 were recorded with a total station. Specifically, the three-dimensional position of the
125 finds was always recorded at the lowest point of contact of the item with the sediment.
126 Dense clouds of surface points of the elephant skeletal elements were acquired using
127 both a total station and a close-range photogrammetric technique.

128 The dimensions (length, width and thickness) of registered finds were measured
129 on-site with millimetre rules. Orientation (plunge and bearing) of elongated particles
130 (i.e., faunal remains, large wood fragments and lithic artefacts) was recorded since
131 2013 using a clock-like system (the bearing was measured, relatively to the grid North,
132 in twelve clockwise intervals of 30°; the plunge with a 22.5° accuracy). In 2015, the
133 use of a compass and inclinometer with an accuracy of 1° was introduced in Area B to
134 gradually replace the former method.

135 The widespread use of a compass and inclinometer to record orientation data (Voorhies,
136 Fiorillo, 1991; Bertran and Texier, 1995; Bertran et al., 1997; Lenoble and
137 Bertran, 2004; Eberth et al., 2007; Eren et al., 2010; Benito-Calvo et al., 2011; Domínguez-
138 Rodrigo et al., 2012; Domínguez-Rodrigo and García-Pérez, 2013; Domínguez-Rodrigo
139 et al., 2014c; Cobo-Sánchez et al., 2014; Organista et al., 2017, among others) was
140 favoured over the alternative use of a total station (Kluskens, 1990; Dibble et al., 1997;
141 McPherron, 2005; Enloe, 2006; Bernatchez, 2010, among others), mostly due to the
142 time-restricted conditions of the rescue excavation conducted at Marathousa 1.

143 Measurements of the bearing (azimuth) and plunge (dip) of elongated finds were
144 taken along the symmetrical longitudinal a-axis (SLA) of elongated bones (Domínguez-
145 Rodrigo and García-Pérez, 2013), lithic artefacts (Bertran and Texier, 1995) and wood
146 fragments (Macdonald and Jefferson, 1985), using the lowest endpoint of the a-axis as
147 an indicator of the vector direction.

148 Other major axes have been alternatively used with the recent application of GIS
149 techniques to retrieve orientation data from secondary source, i.e., from excavation
150 photographs, drawings or maps (Boschian and Saccà, 2010; Benito-Calvo and de la
151 Torre, 2011; de la Torre and Benito-Calvo, 2013; Walter and Trauth, 2013; García-
152 Moreno et al., 2016; Sánchez-Romero et al., 2016). However, the experimental works
153 of Domínguez-Rodrigo and García-Pérez (2013) and Domínguez-Rodrigo et al. (2014c)
154 showed that the SLA, defined as the major axis which symmetrically divide the bone,
155 is more accurate in estimating the flow direction, regardless of bone shape. This a-axis
156 is widely used in taphonomic studies (Toots, 1965; Voorhies, 1969; Eberth et al., 2007;
157 Domínguez-Rodrigo et al., 2012, 2014a; Aramendi et al., 2017, among others) for de-
158 termining the preferential orientation of anisotropic assemblages. The a-axis or major
159 axis of the artefact, measured as the long diameter of the triaxial ellipsoid that approx-
160 imates the particle shape (Krumbein, 1941), is as well used in studies which employ a
161 sedimentological approach to archaeological fabric (Bertran and Texier, 1995; Bertran
162 et al., 1997; Lenoble and Bertran, 2004; Benito-Calvo et al., 2009, among others).

163 The present study focuses on the excavated stratigraphic units in which most of the
164 archaeological and palaeontological remains were recovered in both excavation areas,
165 namely in UA3c and UA4 in Area A, and UB4c and UB5a in Area B. From the total,
166 subset samples of material were used for each specific spatial analysis. For the fabric
167 analysis we included material collected until 2016. For the vertical distribution and
168 point pattern analyses, the region of investigation was limited to the squares excavated
169 from 2013 until 2015, 25 and 29 square meters respectively in each area (Fig. 2).

170 The analyses were performed in R statistical software (R Core Team, 2017). In
171 order to make this research reproducible (Marwick, 2017; Marwick et al., 2017), a
172 repository containing a compendium of data, source code and text is open licensed and
173 available at the DOI: [10.5281/zenodo.822272](https://doi.org/10.5281/zenodo.822272)

174 2.1. Fabric analysis

175 The taphonomic study of the orientation pattern of elongated sedimentary particles,
176 including bones and artefacts, first addressed by Voorhies (1969); Isaac (1967); Bar-
177 Yosef and Tchernov (1972); Schick (1986), more recently led to a noteworthy develop-
178 ment of methods and propagation of applications in Palaeolithic site formation studies
179 (Bertran and Texier, 1995; Bertran et al., 1997; Lenoble and Bertran, 2004; Lenoble
180 et al., 2008; McPherron, 2005; Benito-Calvo et al., 2009, 2011; Benito-Calvo and de la
181 Torre, 2011; Bernatchez, 2010; Boschian and Saccà, 2010; Domínguez-Rodrigo et al.,
182 2012; Domínguez-Rodrigo and García-Pérez, 2013; Domínguez-Rodrigo et al., 2014c;
183 de la Torre and Benito-Calvo, 2013; Walter and Trauth, 2013; García-Moreno et al.,
184 2016; Sánchez-Romero et al., 2016, among others).

185 Fabric analysis can provide valuable insight into site formation and taphonomic
186 processes, allowing discrimination between different orientation patterns (isotropic,
187 linear or planar) possibly associated with a range of sedimentary processes. Whereas
188 water-flow deposits are generally characterised by relatively good sorting and preferred
189 orientation of clasts parallel, or normal to the flow direction (linear fabric) (Petraglia
190 and Potts, 1994); debris-flow deposits mostly exhibit massive, poorly bedded mixtures
191 of unsorted sediments and random orientation of clasts (isotropic fabric), except at the

flow margins where linear fabric may occur (Pierson, 2005). On the other hand, undisturbed archaeological sites, as well as experimental assemblages, have been observed to have planar fabric (Bertran et al., 1997; Lenoble and Bertran, 2004). Nevertheless, grey zones exist between depositional processes, so that an unequivocal discrimination based only on fabric observations is often not possible, and other taphonomic criteria must also be considered (Lenoble and Bertran, 2004). As an example, while overland flows (runoff) have been observed to show some degree of planar fabric (Lenoble and Bertran, 2004), anisotropy without significant transport can be caused in a lacustrine floodplain by low-energy processes such as lake transgression and regression, as well as water-sheet flows formed during rainy seasons (Cobo-Sánchez et al., 2014).

At the margin of a lacustrine environment, relatively close to the surrounding relief, a combination of high- and low-energy processes can be expected. According to the sedimentological and micromorphological study of the Marathousa 1 site, the main find-bearing horizon is associated with hyperconcentrated flows (Karkanas et al., this issue). Hyperconcentrated flows are intermediate states, defined by sediment concentration, in the continuum between sub-aerial water flows and debris flows. Benvenuti and Martini (2002) reported that, when a turbulent hyperconcentrated flow expands over a surface - as in the case of Marathousa 1 - a two-phase flow may develop, with a more concentrated, coarser grained bottom flow-layer (traction carpet) moving slower than the upper turbulent flow-layer carrying wash-load and suspended load. Resultant deposit may exhibit diagnostic inverse grading, or a continuously aggrading bed. Parallel or normal orientation of the clasts to the flow direction can be observed (Benvenuti and Martini, 2002). A simulation model also showed that linear fabric can develop in mud flows. However, after deposition, settling of the clasts may affect the fabric to some extent, depending on the viscosity of the mud flow (Lindsay, 1968).

As part of our three-prong spatial analytic approach, we conducted comparative fabric analysis with the aim to investigate the dynamics of the depositional processes at Marathousa 1. Since fabric strength has been found to be positively correlated with the shape and size of the clast, for the fabric analysis we subset samples of remains with length \geq 2 cm and elongation index (the ratio length/width) $I_e \geq 1.6$ (Lenoble and Bertran, 2004). The samples are listed in Table 1 and include mostly wood fragments and faunal remains from the four stratigraphic units under investigation. Bones have been found to readily react to water flow and show very early anisotropic patterns (Domínguez-Rodrigo et al., 2014c). Flume experiments showed that wood fragments as well tend to align parallel to the current direction (Macdonald and Jefferson, 1985). No distinction of skeletal elements was made, both due to the high fragmentation rate of faunal remains in Area B, and because recent experiments showed a similar orientation pattern for different bone shapes (Domínguez-Rodrigo et al., 2012; Domínguez-Rodrigo and García-Pérez, 2013).

The sample of bones belonging to the individual of *P. antiquus* from Area A was analysed separately and included the humerus, ulna, femur and tibia; the atlas, axis and other 16 complete vertebrae or vertebral fragments; 29 complete ribs or rib fragments; 2 calcanea; 4 metatarsals/metacarpals; the pyramidal; the trapezoid and the pelvis. The sample from UB5a was too small (only 7 observations) and was therefore excluded. In order to assess the reliability of the orientation data recorded using the clock method, we separately analysed two sub-samples from unit UB4c, selected from a set of finds

Table 1: List of sampled observations for the fabric analysis.

Sample	<i>n</i>	Type		
		Fauna	Wood	Lithic
UA3c	49	23	25	1
UA4	38	8	30	-
<i>P. antiquus</i>	63			
UB4c	38	30	1	7

recorded using both methods. All the sampled observations are representative of the whole study area.

Rose diagrams and uniformity tests, such as Rayleigh, Kuiper, Watson and Rao tests (Jammalamadaka et al., 2001), were used to visualise and evaluate circular isotropy in the sample distribution. The Rayleigh test is used to assess the significance of the sample mean resultant length (\bar{R}), assuming that the distribution is unimodal and not bi- or plurimodal. The \bar{R} ranges from 0 to 1: values close to 1 indicate that the data are closely clustered around the mean direction; when the data are evenly spread \bar{R} has a value close to 0. A $p - value$ lower than 0.05 rejects the hypothesis of uniformity with a 95% confidence interval. Kuiper, Watson and Rao are omnibus tests used to detect multimodal departures from circular uniformity. The Kuiper test (Kuiper, 1960) is a rotation-invariant Kolmogorov-Smirnov test statistic for testing the null hypothesis that the empirical distribution function fits a uniform distribution function. The Watson test (Watson, 1961) is instead related to the Cramer-von Mises test. The Rao's spacing test (Jammalamadaka et al., 2001) is based on the idea that in a uniform distribution successive observations should be approximately evenly spaced and it tests deviation from this distribution. For all the tests, results are evaluated against critical values: a result higher than the critical value rejects with confidence the null hypothesis. We applied three omnibus tests since none of them have very high power and some studies suggested that there is no test that is superior to the others under all circumstances (Pewsey et al., 2013).

Randomness testing of three-dimensional data was conducted with the Woodcock S_1/S_3 test (Woodcock and Naylor, 1983). Considering both the plunge and bearing of the oriented items, this method, based on three ordered eigenvalues (S_1, S_2, S_3), is able to discriminate the shape and strength of the distributions. The shape parameter $K = \frac{\ln(S_1/S_2)}{\ln(S_2/S_3)}$ ranges from zero (uni-axial girdles) to infinite (uni-axial clusters). The parameter $C = \ln(S_1/S_3)$ expresses the strength of the preferential orientation, and its significance is evaluated against critical values from simulated random samples of different sizes. A perfect random uniform distribution would have $C = 0$ and $K = 1$.

The Benn diagram (Benn, 1994) adds to the Woodcock test an isotropy ($IS = S_3/S_1$) and an elongation ($ES = 1 - (S_2/S_1)$) index. Like the former method, it is able to differentiate between linear (cluster), planar (girdle) or isotropic distributions. There are no published raw data from actualistic studies on hyperconcentrated flows or other depositional processes affecting the orientation of bones and artefacts deposited on lacustrine floodplains (but see Morton (2004) and Cobo-Sánchez et al. (2014) as pioneer studies on this subject). However, we included in the Benn diagram relevant

Table 2: List of sampled observations for the vertical distribution and point pattern analyses.

Sample	<i>n</i>	Lithic class					Faunal class			
		Debris/chip	Flake	Bone flake	Tool	Core	Indet.	Bone	Tooth	Microfauna
UA3c	279	46	2	-	1	-	1	171	14	44
UA4	61	3	1	-	-	-	-	45	4	8
UB4c	1243	753	154	1	34	6	2	246	28	19
UB5a	101	50	12	-	3	-	-	30	3	3

274 references to published results from observation of fabrics in modern subaerial slope
 275 deposits, i.e., debris flow and runoff ([Bertran et al., 1997](#); [Lenoble and Bertran, 2004](#)).

276 2.2. Vertical distribution

277 The vertical distribution of materials has been long investigated with the aim of
 278 identifying cultural levels, by visually interpreting cross-sectional plots. However,
 279 recent advances in GIS techniques allow to inspect at higher resolution the three-
 280 dimensional distributions of archaeological remains ([McPherron et al., 2005](#); [Anderson](#)
 281 and [Burke, 2008](#), among others).

282 In analysing the vertical dispersion of material at Marathousa 1, we provisionally
 283 assume that a general concentration of unsorted lithic artefacts and faunal remains in
 284 the proximity of the erosional surfaces would support an autochthonous origin of the
 285 assemblages; whereas a homogeneous vertical distribution of remains from the UA3c
 286 and UB4c units would suggest an allochthonous origin, significant transport and subse-
 287 quent re-deposition of the material. Indeed, massive process such as hyperconcentrated
 288 flows, have high erosional power and rather chaotic structure, which may result in in-
 289 verse or normal grading ([Benvenuti and Martini, 2002](#)).

290 In order to estimate the degree of vertical dispersion while controlling for the size
 291 of the archaeological material, dimensional classes were set up following typological
 292 criteria. Lithic artefacts were classified as debris/chips when smaller than a cutoff
 293 length of 15 mm ([Tourloukis et al., this issue](#)). Other classes include flakes, tools and
 294 cores; the latter being the bigger and heavier debitage product. Table 2 summarises
 295 the sample size for each class. Lithic debris/chips constitute the larger part of the
 296 assemblage from UB4c (60%) and UB5a (49%); whereas in Area A they represent
 297 only a moderate percentage in the upper UA3c unit (16%). The very rare presence of
 298 lithic artefacts in the underlying unit UA4 is nevertheless significant. In this unit, the
 299 faunal remains are also found in much lower numbers, their number reduced to one
 300 fourth of those found in UA3c. For the point pattern analysis (see below), we used the
 301 same subset of material for both excavation areas.

302 For Area B, the material recovered from the water-screening was randomly prove-
 303 nanced according to the 5 cm depth of the excavated spit and the coordinates of the
 304 50x50 cm quadrant of the excavation square. Following the same excavation protocol,
 305 the same procedure was applied for the water-screened material of Area A, which was
 306 randomly provenanced according to 3D-coordinates of the 1x1 m excavation square
 307 and 10 cm spit.

308 Since the merely projection of points to virtual profiles is not a suitable method of
 309 analysis in presence of erosional, and thus uneven, geological contacts - such as those

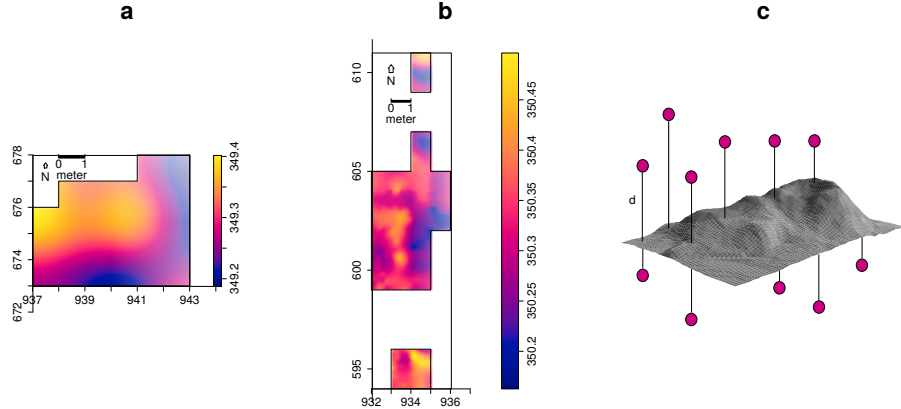


Figure 5: Ordinary Kriging interpolation of the UA3c/4 (a) and UB4c/5a (b) erosional surface; the colour scale denotes absolute elevation in m a.s.l. (c) Illustration of the method used to quantify the vertical dispersion of remains (d) with respect to the UA3c/4 (a) and UB4c/5a (b) surface.

at Marathousa 1, ordinary Kriging interpolation of the recorded points of contact between the UA3c/UA4 and the UB4c/UB5a stratigraphic units were used to reconstruct the UA3c/4 and UB4c/5a erosional surfaces (Fig. 5a,b). In geostatistics, Kriging is a method of interpolation which, from a modelled function of spatial autocorrelation between known points (e.g., recorded elevations), calculates values of unknown points (e.g., predicted elevations). Thus, in order to address our specific objective, i.e., to quantify and analyse the vertical distribution of the archaeological and palaeontological material, we measured the minimum orthogonal distance (d) of each specimen to the interpolated erosional surface (Fig. 5c). For the units above and below this surface (i.e., UB4c and UB5a), the relative distribution of lithic classes and faunal remains was informally tested by means of density estimations.

In Area A, the UA3c/4 erosional contact is locally sharp, but, in contrast to Area B, parts of the eroded unit UA4 are mixed with pockets of the UA3c organic-rich silty sands and intraclast-rich mud flows (Karkanas et al., this issue). However, from sparse known points of the erosional contact, the UA3c/4 surface was interpolated and the vertical dispersion of remains estimated as well. The elephant remains were excluded from this analysis, since they clearly lie horizontally at the UA3c/4 contact (Fig. 4a). Finally, a Student's two sample t-test allowed us to compare the empirical distributions of different groups of remains for each stratigraphic unit.

2.3. Point pattern analysis

A spatial point pattern is defined as the outcome of a random spatial point process (repetitions of it would always create a different pattern). The observed patterns of the archaeological and palaeontological remains were treated as manifestations of spatial point processes, i.e., site formation processes. Point pattern analysis investigates the spatial arrangement of points with the aim of identifying spatial trends. In order to integrate the previous studies of the fabric and vertical distributions, we directed our

336 point pattern analysis equally to the intensity of the patterns (the rate of occurrence of
337 the recorded finds) and to the spatial interaction between different types of finds.

338 As the average number of random points per unit area, intensity informs about
339 homogeneity or inhomogeneity in the distribution of events (e.g., clasts) generated by
340 a point process (e.g., mud flow), i.e., whether the rate of occurrence is uniform or
341 spatially varying across the study area. Intensity, usually non-parametrically evaluated
342 by means of kernel density estimation ([Diggle, 1985](#)), was assessed for the distribution
343 of material from the UB4c, UB5a and UA3c units. Cross-validation bandwidth, which
344 assumes a Cox process, and edge correction were applied using the methods described
345 in [Diggle \(1985\)](#).

346 In the presence of a covariate, it is recommended to further investigate the depen-
347 dence of intensity on that explanatory variable ([Baddeley et al., 2012](#)). In order to
348 evaluate whether variation in the density of materials was correlated to the topography
349 of the erosional surface, we computed a local likelihood smoothing estimate of the in-
350 tensity of remains from UB4c as a function of the UB4c/5a surface elevation model.
351 Formal tests enabled us to assess the evidence of that dependence and to quantify the
352 strength of the covariate. The Kolmogorov-Smirnov test of CSR (Complete Spatial
353 Randomness) and Berman's Z_2 statistics were used to test the strength of evidence for
354 a covariate effect. The Receiver Operating Characteristic (ROC) plot, and the area
355 under the ROC curve (AUC), closely related to Berman's Z_2 test, measure the magni-
356 tude of the covariate effect. AUC values close to 1 or 0 indicate strong discrimination,
357 whereas intermediate values (0.5) suggest no discrimination power.

358 Intensity, evaluated by means of kernel density maps, although informative and
359 widespread in the literature, nonetheless does not provide sufficient information to reli-
360 ably infer about site formation processes. Whereas intensity is a first-order property of
361 the point process, multiscale inter-point interaction is measured by second or higher-
362 order moment quantities, such as the Ripley's K correlation function ([Ripley, 1976,](#)
363 [1977](#)) and the distance G -, F - and J -functions. Three different types of inter-point in-
364 teraction are possible: random, regular or cluster. In a hypothesis-testing framework,
365 point-wise envelopes are computed by a number of random simulations of the null hy-
366 pothesis (i.e., random/Poisson distribution). Thus, values of the empirical distribution
367 (black solid line) are plotted against the benchmark value (red dotted line) and the en-
368 velopes (grey area) which specify the critical points for a Monte Carlo test ([Ripley,](#)
369 [1981](#)). Regular patterns are assumed to be the result of inhibition processes, while
370 cluster patterns are the result of attraction processes.

371 In order to test the spatial interaction between remains associated with the erosional
372 event of UB4c and those associated with the underlying UB5a unit, we treated the data
373 as a multivariate point pattern, assuming that the point patterns in UB4c and UB5a
374 are expressions of two different stationary point processes, i.e., depositional events.
375 We performed a cross-type pair correlation function $g_{ij}(r)$, derivative of the multitype
376 $K_{ij}(r)$ function, which is the expected number of points of type j lying at a distance
377 r of a typical point of type i . The function is a multiscale measurement of the spatial
378 dependence between types i (UB4c) and j (UB5a). Randomly shifting in 199 Monte
379 Carlo permutations each of the two patterns, independently of each other, estimated
380 values of $\hat{g}_{ij}(r)$ are compared to a benchmark value $g_{ij}(r) = 1$, which is consistent with
381 independence or at least with lack of correlation between the two point processes.

In addition to the pair correlation function, the multitype nearest-neighbour $G_{ij}(r)$ function was used to estimate the cumulative distribution of the distance from a point of type i (UB4c) to the nearest point of type j (UB5a). It measures the spatial association between the two assemblages. For the cross-type G -function, the null hypothesis states that the points of type j follow a Poisson (random) distribution in addition to being independent of the points of type i . Thus, in a randomisation technique, when the solid line of the observed distribution ($\hat{G}_{ij}(r)$ or $\hat{g}_{ij}(r)$) is above or below the shaded grey area, the pattern is significantly consistent with clustering or segregation, respectively. In order to reduce the edge effect bias in estimating the correlation between points, we implemented Ripley's isotropic edge correction (Ohser, 1983; Ripley, 1988).

Complete spatial randomness and independence (CSRI) of the two point processes (UB4c and UB5a) would support an allochthonous origin hypothesis for the assemblage recovered from the UB4c unit. According to the allochthonous model, the massive, chaotic UB4c flow event randomly re-elaborated the material entrained in it, independently from the material deposited in UB5a. On the other hand, positive or negative association can be interpreted as expressions of different autochthonous processes.

As for the three-dimensional distribution of the lithic artefacts in Area A, and their spatial association with the partial skeleton of the *P. antiquus*, we applied three-dimensional univariate and bivariate second-order functions. A rectangular box of 20 square meters and 80 cm vertical extent was selected for the analyses (green outline in Fig. 11a). Assuming homogeneity, the univariate pair correlation function $g_3(r)$ was estimated for the pattern of all the artefacts (mostly debris/chips) from UA3c and UA4. In the specific context of the site, complete spatial randomness (CSR) would suggest that the pattern most probably is the result of a random distribution process, such as a high energy mass movement, thus supporting an allochthonous model of deposition. On the other hand, spatial aggregation would support a primary origin of the assemblage. Nevertheless, topography and natural obstructions may generate spatial clustering as well.

In support to the pair correlation function, the cross-type nearest-neighbour function has been applied in order to compute, for each artefact recovered from the UA3c and UA4 units, the nearest point of the three-dimensional clouds of points associated with the elephant skeleton. A prevalence of short distances would indicate aggregation of the lithic artefacts around the mass of the elephant; whereas a uniform or symmetric distribution would support the action of random independent processes.

3. Results

3.1. Fabric analysis

The rose diagrams in Fig. 6 visualise the circular distributions of the examined specimens. Overall, the UA4 sample and the sample of elephant bones show unimodal distributions with predominant peaks in the NE quadrant; while the ones from units UA3c and UB4c suggest multimodal distributions. Specifically, the UA4 sample distribution (Fig. 6b) spreads largely in the NE quadrant. Similarly, the circular distribution of the elephant sample (Fig. 6c), mainly lying in UA4, resembles the former distribution: it is skewed to the SW and concentrated in the NE quadrant. On the other

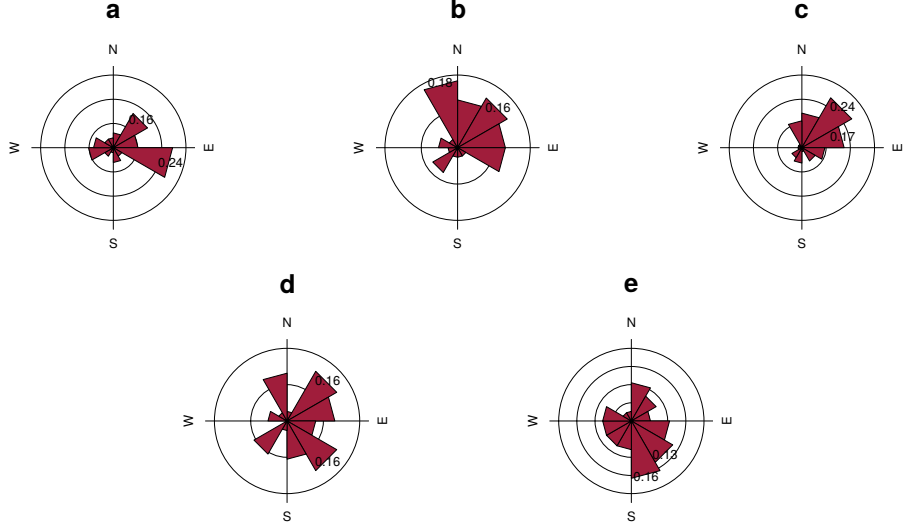


Figure 6: Rose diagrams showing the bearing patterns of samples from UA3c (a), UA4 (b), the elephant carcass (c) and UB4c (d: clock method, e: compass method).

Table 3: Value and p – value of circular uniformity test statistics.

Sample	mean dir.	Rayleigh		Kuiper		Watson		Rao	
		\bar{R}	p	V_n	p	U^2	p	U	p
UA3c	77.17°	0.268	0.029	2.4698	<0.01	0.2967	<0.01	271.8367	<0.001
UA4	35.79°	0.386	0.003	2.5656	<0.01	0.3437	<0.01	246.3158	<0.001
<i>P. antiquus</i>	54.64°	0.489	2.775e-07	3.4811	<0.01	0.906	<0.01	291.4286	<0.001
UB4c (clock)	91.66°	0.276	0.054	1.8963	0.01< p <0.025	0.1937	0.025< p <0.05	255.7895	<0.001
UB4c (compass)	151.17°	0.243	0.106	1.3944	>0.15	0.1268	>0.10	128.5263	>0.10

hand, the UA3c sample (Fig. 6a) shows a bimodal distribution with two peaks to the E and NE, and the two samples from Area B (Fig. 6d,e) suggest a different multimodal scenario uniformly distributed.

Table 3 summarises the results of the circular uniformity tests. With regard to the UA3c sample, the Rayleigh test (p – value = 0.03) rejected the null hypothesis of circular uniformity. The mean resultant length ($\bar{R} = 0.27$) and the mean direction of 77° are thus significant, assuming the distribution is unimodal. However, the rose diagram (Fig. 6a) showed a bimodal distribution. The Kuiper, Watson and Rao omnibus tests, more powerful than the Rayleigh test in detecting multimodal deviation from uniformity, also rejected the null hypothesis of uniformity, therefore suggesting significant anisotropy in the distribution. For the UA4 sample and the subset of elephant bones, all the uniformity tests agreed in rejecting the null hypothesis in favour of a preferentially oriented distribution. The elephant sample, with respect to the other, showed significantly higher test results, thus stronger anisotropy. As suggested by the rose diagrams (Fig. 6c), this sample has a mean direction towards the NE (55°) and relatively low circular variance (29°).

The UB4c sub-samples had discordant test results when considering the omnibus

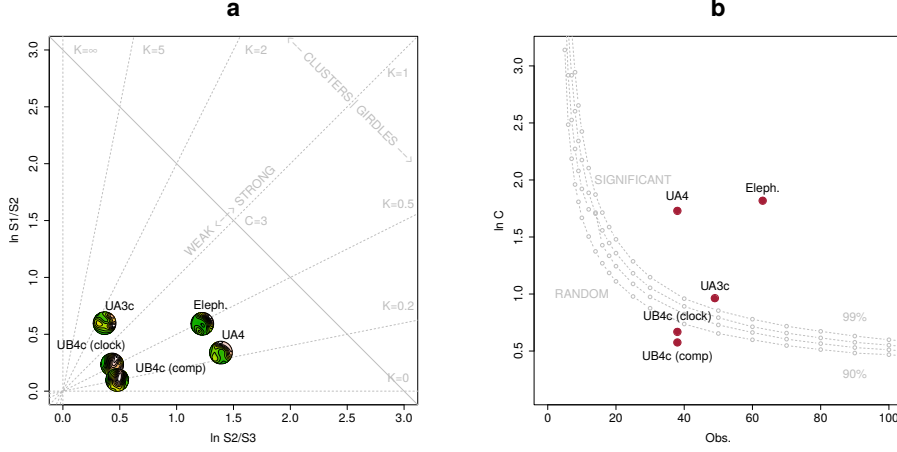


Figure 7: Woodcock's eigenvalues ratio graph (a) and plot of the Monte-Carlo critical S_1/S_3 test values, for varying sample sizes and confidence levels (b), modified from [Woodcock and Naylor \(1983\)](#).

442 statistics. However, according to the Rayleigh test, the mean resultant lengths (\bar{R})
 443 and the mean directions were not significant for both sub-samples of measurements:
 444 $p - values > 0.05$ failed to reject the null hypothesis of isotropy with 95% confidence
 445 interval. This result is well confirmed by the Kuiper, Watson and Rao tests for the
 446 sub-sample of measurements recorded using the compass. Conversely, the omnibus
 447 tests failed to reject the hypothesis of uniformity for the other sub-sample of measure-
 448 ments recorded with the clock method. The rose diagram (Fig. 6d) suggested for the
 449 latter distribution strong multimodality, with uniformly spread peaks. The contrasting
 450 results obtained for the UB4c sub-samples are most probably due to the shape of those
 451 distributions. Indeed, the clock system, being less accurate, tends to produce a less
 452 dense distribution, more subject to show a multimodal shape when the distribution is
 453 actually uniform.

454 The Woodcock eigenvalues ratio graph (Fig. 7a) presents the shape (K) and strength
 455 (C) of the distributions. Fig. 7b plots confidence levels of Monte-Carlo critical C val-
 456 ues, varying for sample sizes. The two sub-samples from Area B nearly overlapped,
 457 thus suggesting reliability of the orientation measurements collected using the clock
 458 system, although of low accuracy. The two sub-samples, together with the UA3c sam-
 459 ple, having low C values, plotted close to the origin of the ratio graph. Therefore, they
 460 indicate weak preferential orientation (UA3c) and significant randomness (UB4c). On
 461 the other hand, the UA4 and the elephant samples, with higher C values, showed a
 462 stronger and significant tendency to orient preferentially. The shape parameter K of
 463 the samples varied from $K = 0.25$ for the UB4c sample measured with the compass,
 464 to $K = 0.66$ for the one measured with the clock, to $K = 0.48$ for the elephant sample.
 465 Overall, all the samples, except the UA3c one ($K = 1.63$), plotted below the average
 466 shape value ($K = 1$) between girdles and clusters distributions.

467 The Benn diagram (Fig. 8) resembles the Woodcock ratio graph (Fig. 7a). The
 468 samples from units UB4c and UA3c clearly plotted at a distance from the UA4 and

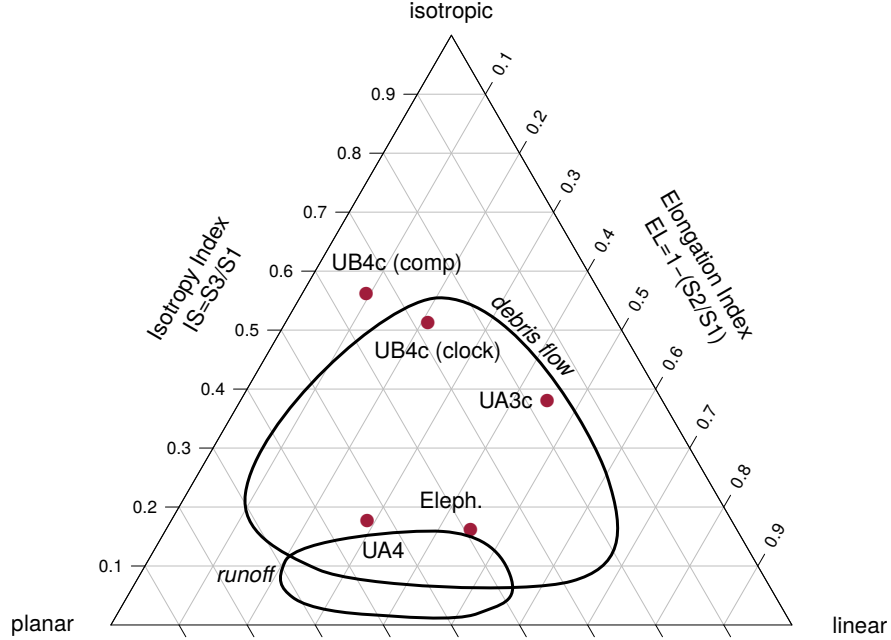


Figure 8: Benn's diagram. Fabric ranges of natural processes modified from [Lenoble and Bertran \(2004\)](#).

the elephant samples. The UB4c samples plotted in the upper corner of the ternary graph, with the UB4c sub-sample of measurements taken with the compass exhibiting more isotropy. The UA3c sample, with an elongation index similar to the elephant sample, but higher isotropic index, plotted towards the centre. Compared to the ranges of fabrics recorded for modern natural processes (debris flow and runoff), the fabric from the UA3c and UB4c units plotted well inside the cluster of debris flows, with the UB4c (comp) sample suggesting even more random orientations. On the other hand, the sample of elephant remains, which lie mostly on UA4 and are covered by UA3c, plotted significantly close to the sample from unit UA4. They both presented the lowest isotropy index (IS), but not high elongation index (EL). Thus, they plotted in the average between linear and planar orientations, at the margins of the range of runoff processes. Yet they still plotted within the cluster of debris flows fabrics. Moreover, as suggested also by the uniformity tests (Tab. 3), the elephant sample showed a more linear attitude with respect to the UA4 sample.

3.2. Vertical distribution

Fig. 9 compares the vertical distribution of the finds from units UA3c and UA4, by means of empirical density functions of the minimum distances (d) from each specimen to the UA3c/4 erosional contact (Fig. 5a). Three lithic artefacts (two flakes and one tool) from the UA3c unit, not included in Fig. 9, plotted within 15 cm from the interpolated surface. Only one flake has been found in the lower UA4, at about 17 cm

489 from the UA3c/4 contact, together with three chips. Despite the scarcity of debitage
490 products in this area, waste products (debris/chip) are relatively well represented (16%
491 of the UA3c sample). Their vertical dispersion approximated a normal distribution
492 ($\mu = 0.24$, $\sigma = 0.15$): the Kolmogorov-Smirnov and Shapiro tests failed to rejected
493 the null hypothesis of normality ($p - value = 0.83$ and 0.075, respectively). Notably, the
494 distributions of the faunal remains from the same unit UA3c were all right skewed, with
495 means (μ) about 20 cm above the UA3c/4 contact. Nevertheless, the Welch two sample
496 t-test ($p - value = 0.61$) failed to reject the null hypothesis that the lithic and faunal
497 sample means are equal. The total distribution of remains from unit UA3c showed a
498 unimodal distribution, skewed to the right, with mode in the proximity of the UA3c/4
499 surface. Similarly, the vertical distribution of faunal remains recovered from unit UA4
500 concentrate in the first 10 cm below surface. The density functions altogether clearly
501 confirmed one of the main observations assessed during excavation, namely that, with
502 the elephant remains lying at the UA3c/4 contact and covered by unit UA3c, most of the
503 faunal and lithic material were recovered from unit UA3c (Fig. 2) and predominantly
504 in the proximity of the UA3c/4 contact (Fig. 9).

505 Fig. 10 shows the empirical density functions of the minimum distances from each
506 specimen from Area B to the UB4c/5a erosional contact (Fig. 5b). The combined
507 distribution of any type of find from the UB5a unit (Fig. 10a) skewed to the left with
508 a short tail (up to -0.3 m). The mode, between 5 and 10 cm below the roof of UB5a,
509 indicates a general concentration of material very close to the contact of this unit with
510 the overlying UB4c, in accordance with the mean distribution of the different classes of
511 remains. Although the majority of both the lithic and faunal assemblages were found
512 in the uppermost 15 cm of UB5a, few debris/chips and bone fragments occur lower
513 in the sequence, yet no more than 30 cm below the roof of this unit. Very few flakes,
514 three tools and no cores have been found in this unit. As a whole, the lithic assemblage
515 from UB5a, mostly composed by debris/chips, is only 7% of the most conspicuous
516 assemblage from UB4c.

517 The global distribution of unit UB4c was right skewed (up to almost 0.6 m) and
518 centred at about 5 cm above the contact with the underlying unit UB5a (Fig. 10b).
519 Almost 30% of the sample fell exactly at the erosional contact that separates UB4c
520 from UB5a. The density estimations of the lithic debris/chip, flakes, tools and faunal
521 remains significantly overlap, whereas the distribution of the six cores shows a bimodal
522 shape with peaks at 5 and 20 cm above the contact. Moreover, the Welch Two Sample t-
523 test of the lithic and faunal sample means failed to reject the null hypothesis ($p-value =$
524 0.6295).

525 3.3. Point pattern analysis

526 Results of the point pattern analysis are complementary to those obtained from
527 the analysis of the fabric and vertical distributions. Regarding Area A, kernel den-
528 sity estimation and three-dimensional functions were applied in order to quantitatively
529 depict the spatial distribution of the lithic assemblage in relation to the elephant skele-
530 ton. Fig. 11a shows the smoothing kernel intensity estimation of the faunal assemblage
531 from the UA3c unit. Contour lines delimit the density of the lithic sample. The partial
532 skeleton of the *P. antiquus* is superimposed on it. A preliminary visual examination
533 of the plot suggests a homogeneous distribution of lithics (mostly debris/chips) and

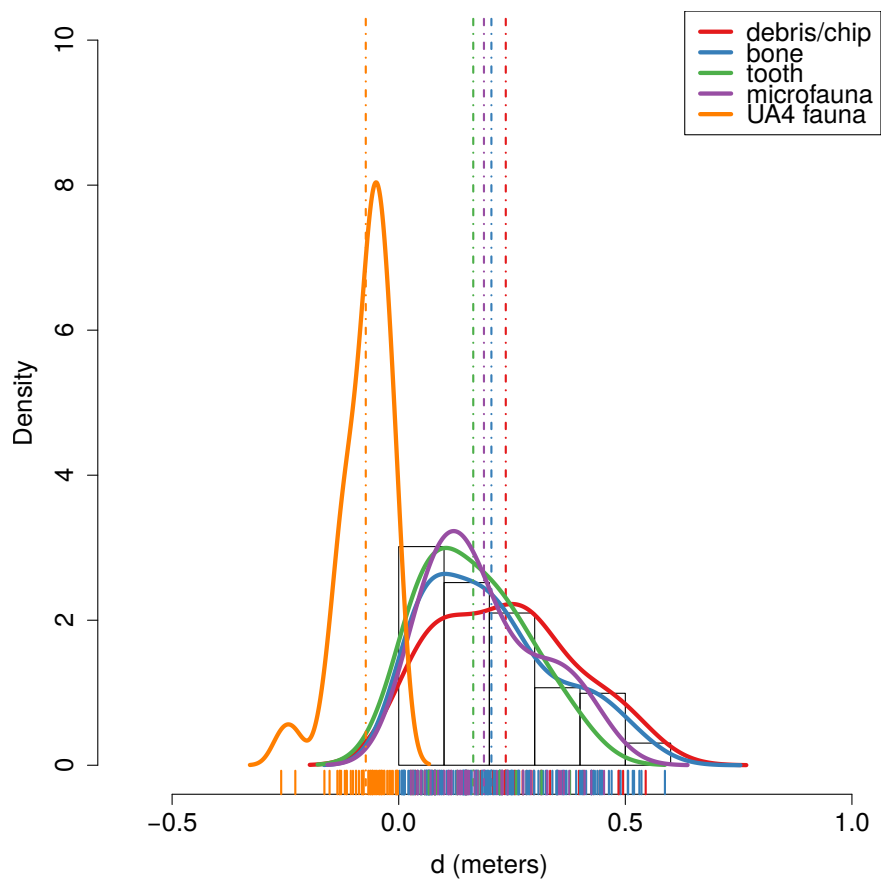


Figure 9: Empirical density functions of minimum orthogonal distances (d) to the UA3c/4 surface. The histogram represents the total distribution of remains from UA3c; dashed lines indicate mean values.

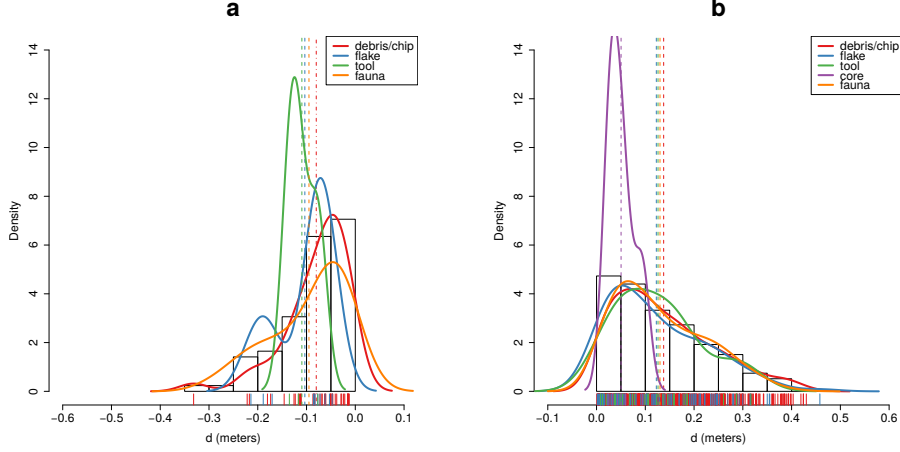


Figure 10: Empirical density functions of minimum orthogonal distances (d) to the UB4c/5a surface. The histogram represents the total distribution of remains from UB5a (a) and UB4c (b); dashed lines indicate mean values.

fossils. Spots of higher density appear to be spread around and in association with the elephant remains.

The univariate pair correlation function of the joined lithic assemblage from the UA3c and UA4 units (Fig. 11b) suggests aggregation of finds. The estimated $\hat{g}_3(r)$ function (black solid line) wanders above the benchmark value (red dotted line) until values of $r = 0.8$. However, for distances between 35 and 65 cm, it lies above the grey envelope of significance for the null hypothesis of CSR, indicating that at those distances artefacts occur significantly closer than expected in the case of random processes. For values of $r > 0.8$, the function stabilises at values close to 0, suggesting a Poisson distribution. The plot illustrates the random distribution of finds between patches of clusters that we observe in Fig. 11a.

The histogram in Fig. 11c shows the density of the distances calculated from each artefact to the nearest-neighbour elephant remain. A right skewed distribution, with a prevalent peak at 10 cm and mean (μ) 30 cm is an indication of the relatively strong aggregation of lithics around the mass of the elephant skeleton.

As for Area B, the analysis focused on the spatial distribution and cross-correlation of the assemblages from UB4c and UB5a. Figs. 12a,b respectively show kernel density estimations of the combined lithic and faunal assemblages from both the units analysed. Despite the samples size difference, a first visual examination suggests the presence of interesting spatial structures. Regarding the UB4c unit (Fig. 12a), the high density of material concentrated around the western square 934/600 suggests that the pattern could have been the result of an inhomogeneous, non-uniform depositional process. Visual comparison of the density plot with the elevation model of the erosional contact between the UB4c and UB5a units (Fig. 5b) suggests positive correlation between lower elevations (topographic depressions) and higher density of remains.

Fig. 12c shows the results of the ρ -function, which estimates the intensity of the

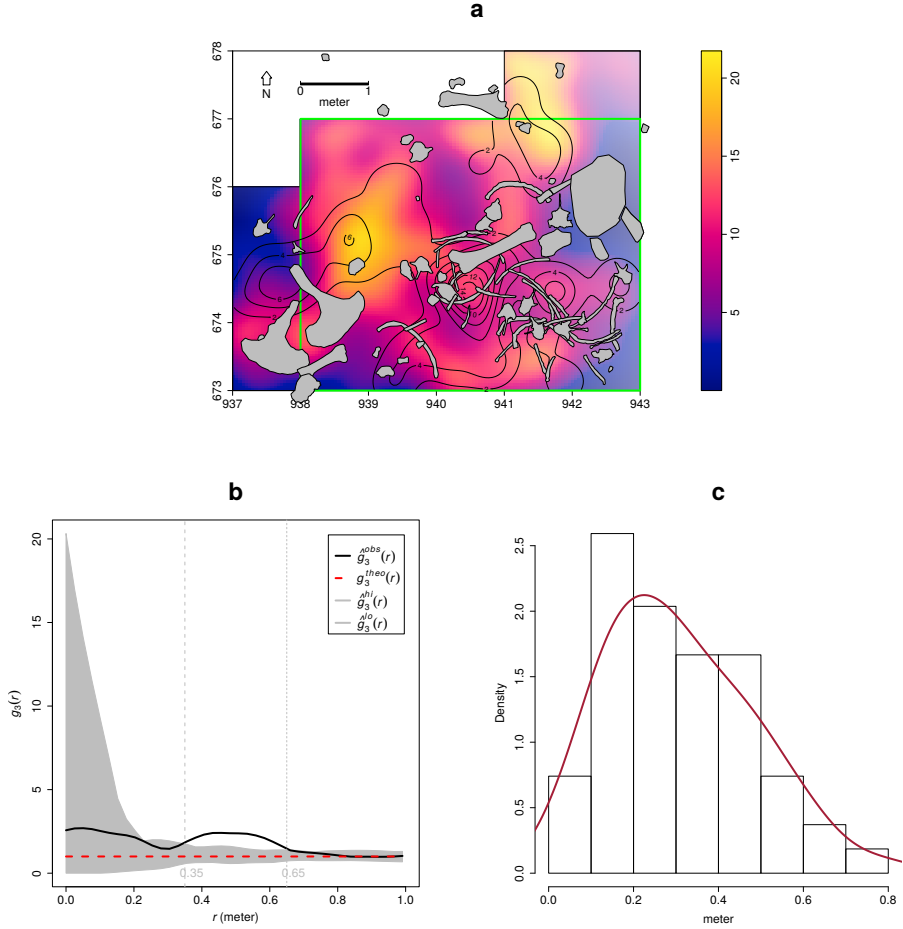


Figure 11: Kernel smoothed intensity function of the faunal assemblages from UA3c. Isolines mark the density of the lithic artefacts from UA3c (a). Pair correlation function ($g_3(r)$) of a three-dimensional pattern of lithic artefacts from UA3c and UA4. Grey envelope of 999 Monte Carlo simulations under the CSR null hypothesis (b). Three-dimensional distance from each lithic artefact from UA3c and UA4 to the nearest neighbour elephant remain (c).

560 UB4c sample assemblage as a function of the covariate underlying topography created
561 by the erosional event. Within the range of elevation between 350.2 and 350.4 m, the
562 occurrence of finds is higher and the intensity decreases with the rise of elevation, i.e.,
563 finds are more likely to be found at lower elevations than would be expected if the
564 intensity was constant. Spatial Kolmogorov-Smirnov (KS) and Berman's Z_2 (Berman,
565 1986) statistics were used in order to test the dependence of the UB4c pattern on the
566 covariate erosional surface. Both KS ($D = 0.11952$, p -value = $7.772e - 16$) and Z_2
567 ($Z_2 = -7.8447$, p -value = $4.34e - 15$) significantly rejected the null hypothesis of
568 CSR. Although the tests suggested evidence that the intensity depends on the covariate,
569 the effect of the covariate is weak and it seems to have no discriminatory power. The
570 ROC curve and AUC statistics (0.56), which measure the strength of the covariate
571 effect, suggest that the underlying UB4c/5a topography does not completely explain
572 the localised high density of occurrence in the UB4c.

573 Relative spatial segregation seems to occur between the assemblages from UB4c
574 (Fig. 12a) and UB5a (Fig. 12b), with high density of the former distribution corre-
575 sponding to low density of the latter. The former analysis of the vertical distribu-
576 tion showed that the two assemblages occur very close to their stratigraphic contact
577 (Fig. 10). In order to further investigate the spatial interaction between the two de-
578 positional events, we applied multitype pair correlation $g_{ij}(r)$ and nearest-neighbour
579 $G_{ij}(r)$ functions. Fig. 12d shows the estimated values of the multivariate $\hat{g}_{ij}(r)$ function
580 against the envelope of the null hypothesis, obtained by randomly shifting the posi-
581 tion of remains from the two distributions in 199 Monte Carlo simulations. For fixed
582 values of r less than 30 cm the observed function lies below the benchmark value of
583 independence, thus indicating segregation; but it wanders at the lower edge of the grey
584 envelope. For fixed distances of $r > 0.3$ m the observed and theoretical lines signifi-
585 cantly overlap. Overall, the function suggests independence of the two point processes
586 (UB4c and UB5a) at multiple scales. However, the estimated $\hat{G}_{ij}(r)$ function (Fig. 12e),
587 running well below the significance grey envelope for fixed values of $r > 0.3$ m, con-
588 firms that the nearest-neighbour distances between remains from UB4c and UB5a are
589 significantly longer than expected in the case of independent processes. Interestingly,
590 at values of $r < 0.2$ m the observed function failed to reject the null hypothesis of
591 Complete Spatial Randomness and Independence (CSRI).

592 4. Discussion

593 Recent excavations at the Middle Pleistocene site of Marathousa 1 have unearthed
594 in one of the two investigated areas (Area A) a partial skeleton of a single individual
595 of *Palaeoloxodon antiquus*, whose bones are in close anatomical association, and spa-
596 tially and stratigraphically associated with lithic artefacts and other faunal remains. In
597 Area B, 60 m to the South of Area A, we collected a much higher number of lithic
598 artefacts (Tourloukis et al., this issue), spatially and stratigraphically associated with
599 other faunal remains, including isolated elephant bones, cervids and carnivores among
600 others (Konidaris et al., this issue). The two areas are stratigraphically correlated, the
601 main fossiliferous layers (UA3c and UB4c) representing a massive depositional pro-
602 cess, such as a hyperconcentrated flow that dumped material in a lake margin context

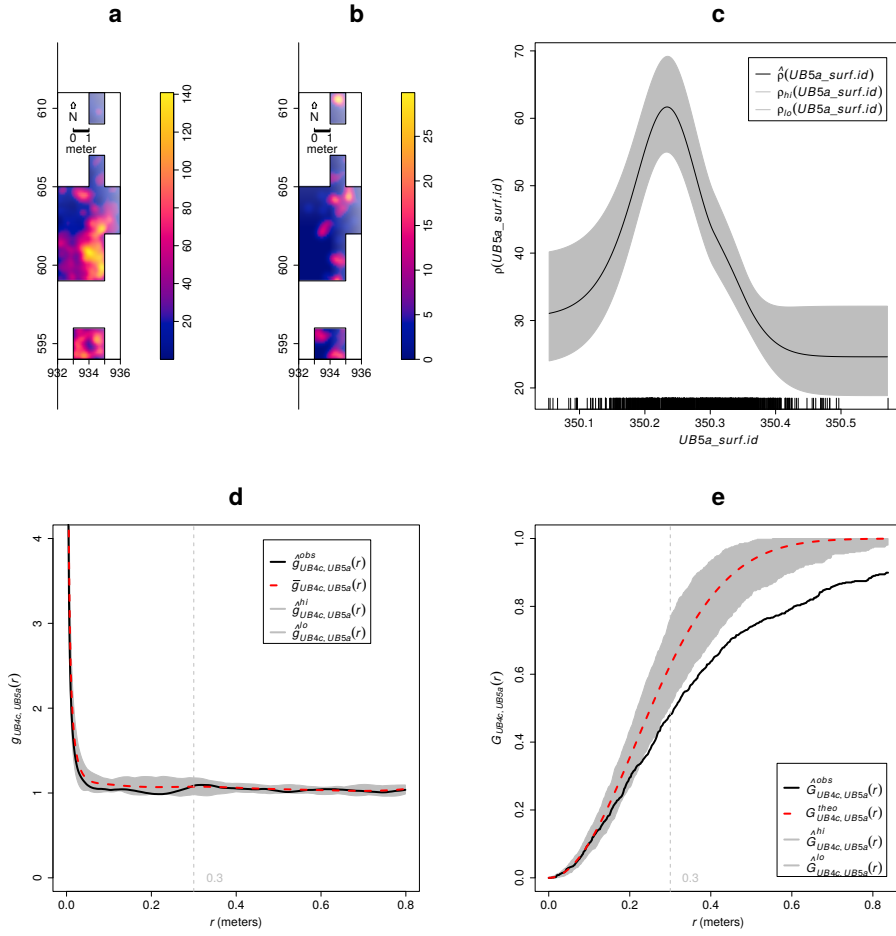


Figure 12: Kernel smoothed intensity function of the lithic and faunal assemblages from UB4c (a) and UB5a (b). Smoothing estimate of the intensity of remains from UB4c, as a function of the erosional surface UB4c/5a. Grey shading is point-wise 95% confidence bands (c). Cross-pattern pair correlation function ($g_{ij}(r)$) between the UB4c and UB5a distributions. Grey envelope of 199 Monte Carlo simulations under the independence of components null hypothesis (d). Multitype nearest-neighbour function ($G_{ij}(r)$) between the UB4c and UB5a distributions (e).

(Karkanas et al., this issue). To date, evidence of butchering (cut-marks) has been identified on two bones of the elephant skeleton from Area A, as well on elephant and other mammal bones from Area B (Konidaris et al., this issue).

However, due to the secondary depositional nature of the main fossiliferous horizon, it is of primary importance to evaluate the degree and reliability of the spatial association of the lithic artefacts with the faunal remains, and especially with the elephant skeleton. In order to tackle our main objective, we applied a comprehensive set of spatial statistics to the distributions of the archaeological and zooarchaeological/palaeontological remains from relevant stratigraphic units of the two areas of investigation. Preliminary results of our analyses are here discussed for both areas.

4.1. Fabric analysis

The analysis of the orientation (plunge and bearing) of subsets of remains, mostly bone, wood fragments and lithic artefacts, showed different patterns for the two main find-bearing units. In Area B, two sub-samples from the same stratigraphic unit were analysed, in order to assess the reliability of the orientation data measured with the clock system. Due to the different shapes of the distributions (Figs. 6d,e), test statistics reported contrasting results (Tab. 3). Indeed, the clock system, recording non-continuous circular data, tends to produce a distribution more subject to show a multimodal shape when it is actually uniform. However, the two sub-samples nearly overlapped when plotted in the three-dimensional Woodcock (Fig. 7) and Benn (Fig. 8) diagrams, thus suggesting some degree of reliability of the clock method. Nevertheless, despite minor differences between the two samples, caution should be paid in analysing grouped circular data.

The test results (Tab. 3) for the UA4 sample and the sample of elephant remains - which lie on unit UA4 and are covered by UA3c - indicated significant preferential orientations towards the NE (Figs. 6b,c). As shown by the Woodcock's (Fig. 7) and the Benn's diagrams (Fig. 8), these samples plotted together at a distance from the others. Such convergence suggests that the elephant carcass, the other faunal remains and the organic material, deposited on unit UA4, were subject to the same processes. Far from the isotropic corner in the Benn's diagram these two samples from Area A plotted approximately in between the linear and planar extremes, with the elephant sample showing a more linear fabric. When the results published by Bertran et al. (1997) and Lenoble and Bertran (2004) from observations of fabrics in modern subaerial slope deposits were used as a reference, the two samples aggregated at the extreme margins of runoff processes. Yet, they plotted well within the cluster of debris flows and relatively distant from the linear corner.

Although Bertran et al. (1997) studied runoff deposits from different environments (channel-lag gravels in rills, small gullies, and inter-rill surfaces on alpine slopes; and faintly laminated gravel lenses on an inactive, small colluvial fan), this result is consistent with the exposure of unit UA4 to overland water-laden processes that occurred before the flood event UA3c/UB4c. Notably, the erosive nature of low-energy processes triggered by rain-water has been observed on lacustrine floodplains, and is associated with anisotropic patterns in autochthonous assemblages (Cobo-Sánchez et al., 2014; Domínguez-Rodrigo et al., 2014c; García-Moreno et al., 2016).

647 Pockets of thinly bedded organic-rich silty sands have been found mixed in UA4.
648 These sands in Area A resemble the UB5b/c sandy deposit in Area B, which is associated
649 with relatively high energy fluvial flows entering the lake margins ([Karkanas et al., this issue](#)). Eventually, such relatively high energy flood (UB5b/c) would have had the
650 power to significantly reorient elements of the elephant carcass and slightly displace
651 them. However, the elephant skeleton clearly lies on top of unit UA4 and is covered by
652 UA3c (see Fig.4).

653 Moreover, unlike bones with a tubular shape (i.e., long bones), ribs and vertebrae
654 are prone to orient preferentially under high energy processes, less likely under low
655 energy processes ([Domínguez-Rodrigo and García-Pérez, 2013; Domínguez-Rodrigo et al., 2014c](#)). Interestingly, whereas some of the ribs share the same preferential orientation
656 with the long bones, others are oriented NW/SE. However, a NW/SE orientation
657 could be consistent with a prevalent NE direction of the flow (and vice-versa), since
658 long bones could roll orthogonally to the flow direction ([Voorhies, 1969](#)). On the other
659 hand, a higher energy flood would lead to an under-representation of skeletal elements
660 with FTI (Fluvial transport Index) values ≥ 75 (sacrum, patella, astragalus, calcaneum,
661 cervical, thoracic and lumbar vertebrae), which are more prone - when disarticulated
662 - to be easily transported by water induced processes ([Frison and Todd, 1986](#)). Yet,
663 several of these bones are present and in close spatial association with the elephant
664 cranium and other skeletal elements. The presence of many of the skeletal elements
665 with different transportation properties suggests that the elephant carcass was not subjected
666 to high energy processes (and probably still articulated) before the flood event
667 UA3c/UB4c.

668 The fabrics of the UA3c and UB4c samples, with higher isotropic index (*IS*), plotted
669 at a significant distance from the elephant sample, yet within the cluster of debris
670 flows (Fig. 8). Indeed, random distribution and orientation of clasts is expected for debris
671 flows, except at flow margins, where preferential orientation and clusters of clasts
672 have been observed ([Pierson, 2005](#)). However, hyperconcentrated flows, such as the
673 UA3c/UB4c flood event, which fall in between the spectrum of water and debris flows,
674 may develop parallel or normal orientation to the flow direction ([Lindsay, 1968; Ben-](#)
675 [venuti and Martini, 2002](#)). Notably, with respect to the UB4c sample, the UA3c sample
676 exhibits a higher elongation index (*ES*), similar to that of the elephant sample (Fig. 8).
677 Rose diagrams (Fig. 6) and uniformity tests (Tab. 3) also suggest similar fabrics of the
678 samples from Area A.

679 Thus, we can assume that an overland flow, namely UA3c/UB4c, is likely to have
680 slightly reworked and preferentially oriented to the NE the exposed elements of the
681 already dismembered (and probably already marginally displaced) elephant carcass,
682 which mostly preserves close anatomical associations, but not anatomical connections.
683 Although little is currently known about the spatial extension of the UA3c/UB4c flow
684 event, the different orientation patterns between the two areas could probably be ex-
685 plained with lateral variability. Indeed, the same event could exhibit different be-
686 haviours at different temporal and spatial points, giving rise to different distribution
687 patterns. However, as suggested by [Lenoble and Bertran \(2004\)](#), fabric analysis is not
688 sufficient to unequivocally discriminate processes and should therefore be integrated
689 with the analysis of other diagnostic features.

692 4.2. Vertical distribution

693 As for the vertical distribution, we assumed that mass processes, such as hypercon-
694 centrated flows, would predominantly distribute poor to very poor sorted clasts homo-
695 geneously throughout the sequence (Pierson, 2005). Diagnostic inverse grading, or a
696 continuously aggrading bed can be observed in the resultant deposits (Benvenuti and
697 Martini, 2002). A concentration of unsorted elements in the proximity of the erosional
698 surface, as well as the absence of any grading, would in turn suggest an autochthonous
699 assemblage.

700 The lithic assemblage from Area A - the combined units UA3c and UA4 ($n = 54$),
701 composed by a few debitage products and a relatively high number of debris/chips
702 and retouch waste products (Tab. 2) - plotted predominantly in the proximity of the
703 erosional surface created by the UA3c/UB4c event (Fig. 5a). The faunal remains from
704 unit UA3c resemble the distribution of the archaeological assemblage; whereas the
705 ones from the underlying unit UA4 plotted within 10 cm below the erosional contact.
706 Overall, the material recovered from unit UA3c did not show any grading and mainly
707 plotted at the bottom of the unit (Fig. 9). Thus, its vertical distribution is consistent
708 with the hypothesis of an autochthonous assemblage.

709 In Area B, two samples from units UB4c ($n = 1243$) and UB5a ($n = 101$) respec-
710 tively, were analysed (Tab. 2) for quantifying the minimum orthogonal distance of each
711 item to the modelled erosional surface (Fig. 5b). The vertical distribution of lithic arte-
712 facts and fossils from unit UB4c showed a predominant peak right at the contact with
713 the erosional surface. Almost 30% of this rich sample plotted at a distance between 0
714 and 5 cm from the erosional contact; whereas the rest gently skewed to the upper part
715 of the unit, up to about 50 cm. The same distribution was observed for all classes of
716 remains, suggesting no size sorting and an origin very close to the erosional surface
717 (Fig. 10b).

718 The density distribution of the sample from the underlying UB5a unit (Fig. 10a)
719 globally indicates a more constrained vertical displacement of remains (within 30 cm
720 below the erosional surface). Whereas lithic artefacts and fossils mostly plot right at
721 the contact and just below it, a few debris/chips and faunal remains were found lower
722 in the sequence. No size sorting was observed, but, notably, lithic cores are absent and
723 the debris/chip distribution is wider than the distribution of the few flakes and tools.
724 Field observations of cracks in the clayey UB5a unit testify to shrinking and swelling
725 during wet and dry cycles (Karkanas et al., this issue), which suggests that vertical dis-
726 placement of some small lithics and fossil fragments at lower depths with respect to
727 the UB5a/4c contact probably resulted from clay desiccation. Likewise, Lenoble and
728 Bertran (2004) documented up to 30 cm vertical dispersion and frequent vertical plunge
729 of artefacts from the marshy silty clay of the Croix-de-Canard site, sector 3. Further-
730 more, a recent experimental study of animal trampling in water saturated substrates
731 reported negative correlation with artefact size, significant inclination and greater ver-
732 tical displacement than any former work: a maximum between 16 and 21 cm, with a
733 mean of about 6 cm (Eren et al., 2010).

734 The fact that the majority of the remains from units UB4c and UB5a plotted at, or
735 very close to the contact between these two layers, the relatively high percentage of
736 lithics in both units, as well as the absence of grading, suggest autochthonous assem-

737 blages, deposited in UB5a and subsequently eroded *in situ* by the UA3c/UB4c flood
738 event.

739 **4.3. Point pattern analysis**

740 The autochthonous hypothesis was further explored by means of point pattern
741 analysis. According to this model, in both areas the lithic and faunal assemblages
742 were primarily deposited *in situ* and were subsequently eroded and re-deposited (*sensu*
743 Fernández-López, 1991) by the hyperconcentrated flow UA3c/UB4c. We assumed
744 that a completely random spatial distribution of the lithic artefacts and faunal remains
745 would suggest an allochthonous origin and subsequent re-elaboration (*sensu* Fernández-
746 López, 1991), with transport to the site by the action of a random massive process.
747 Nevertheless, clustering of artefacts is not necessarily evidence of human presence.
748 Aggregation or segregation patterns could be produced by a range of biotic and/or nat-
749 ural processes. Human activities, topography and physical obstructions alike could
750 trigger spatial aggregation.

751 The three-dimensional distribution of lithic artefacts from unit UA3c shows signif-
752 icant clustering for values of r between 35 and 65 cm. Lithic artefacts occur relatively
753 close to the skeletal elements of the elephant, at a distance between 20 and 50 cm at
754 most (Fig. 11). The richest cluster of about 20 lithic artefacts is located to the SW of the
755 cranium, close to the right femur and the scatter of ribs and vertebrae. Considering the
756 prevalent NE orientation of the elephant bones and the other faunal remains from UA4
757 and UA3c, it is not unlikely that a SW/NE oriented flood could have been responsible
758 for the observed accumulation to the SW of the elephant cranium, which would have
759 represented an important obstruction to the flow. A similar case of clustering of small
760 remains, apparently dammed by a long elephant tusk, has also been observed at Castel
761 di Guido (Italy) by Boschian and Saccà (2010). Secondary deposition by low-energy
762 flows and clustering of artefacts and bones blocked by an aurochs carcass have been
763 as well documented at the site of 'Ein Qashish (Israel) (Hovers et al., 2014). However,
764 the pair correlation function (Fig. 9b) suggests significant clustering of lithic artefacts
765 at relatively small scale: a pattern less likely to be produced by a large scale massive
766 process such as a hyperconcentrated flow. Moreover, clusters of lithic artefacts occur
767 as well in areas with lower densities of elephant bones.

768 Small scale clustering; proximity to the elephant remains and the erosional sur-
769 face; absence of spatial size sorting and, on the contrary, the presence of a relatively
770 high number of lithic debris/chips associated with some flakes, tools and a rich fau-
771 nal assemblage; close anatomical spatial association of the elephant skeletal elements,
772 slightly displaced and preferentially oriented: altogether these lines of evidence support
773 the hypothesis of an autochthonous deposition, subject to localised minor reworking.

774 A similar pattern can be observed in Area B, where an initial set of spatial statistics
775 confirmed that the inhomogeneous density of remains from unit UB4c (Fig. 12a) is
776 not completely explained by the covariate effect of the underlying complex topography
777 created by the erosional event UA3c/UB4c (Fig. 5b). Thus, we explored the relative
778 spatial interaction between the UB4c and the underlying UB5a samples. We assumed
779 that complete spatial randomness of the two independent depositional processes would
780 occur in case of an allochthonous origin and transportation of the UB4c assemblage.

781 The hypothesis of an autochthonous original deposition of the faunal and lithic as-
782 semblages on the UB5a unit, subsequently eroded *in situ* by a relatively high energy
783 flood (UB4c), was tested by cross-pattern spatial correlation functions (Figs. 12d,e).
784 Whereas the two samples are vertically adjacent to the erosional surface (Fig. 10), on
785 the horizontal plane they are both more segregated than expected for a random distri-
786 bution.

787 Conversely, the extraordinary preservation and number of mint to sharp, unsorted
788 lithic artefacts from the UB4c unit; their density, positively correlated to the topog-
789 raphy, and significantly segregated from the underlying distribution of remains; the
790 vertical proximity of both assemblages from UB4c and UB5a to the erosional surface;
791 as well as the random orientation pattern of the former, suggest that significant dis-
792 placement of materials due to the erosional event can be excluded. The faunal and
793 lithic assemblages from unit UB4c therefore most likely derived from the local erosion
794 of exposed mudflat areas (unit UB5a) and have been slightly redistributed by the same
795 flood event that capped the elephant in Area A.

796 Further evidence that the recovered assemblage has not undergone substantial re-
797 working and has retained its original characteristics would come from the refitting anal-
798 ysis, currently in progress. To date, 4 bone refits have been found in Area B: three from
799 unit UB4c, respectively at 4.77, 0.05 and 0.01 m distance; and one between two mam-
800 mal bone fragments from units UB4c and UB5a, at a very short distance (0.09 m).
801 Interestingly, one of the elements of the most distant refit (a *Dama* sp. mandibular
802 fragment) shows traces of carnivore gnawing (Konidaris et al., *this issue*).

803 In conclusion, multiple lines of evidence reject an allochthonous hypothesis of de-
804 position in favour of an autochthonous model. The erosional event UA3c/UB4c repre-
805 sents an *en masse* depositional process, i.e. a hyperconcentrated flow, in the continuum
806 between water and debris flow, which would have locally reworked at a small scale
807 the already exposed or slightly buried and spatially associated lithic and faunal assem-
808 blages.

809 Although the UA3c/UB4c process represents a snapshot of a relatively short time-
810 frame, high resolution inferences about the use of space by human groups, in terms
811 of knapping episodes and butchering activities, are unreliable in light of the current
812 information. The spatial pattern observed at the site is indeed the result of the last
813 episode in a palimpsest of spatial processes. Whereas the erosional event represented
814 by the hyperconcentrated flow UA3c/UB4c caps the fossiliferous horizon and preserves
815 the record, little is known about the underlying, eroded 'occupational' surface.

816 However, whereas hunting or scavenging in the Lower Palaeolithic is still an un-
817 solved matter of debate, considering the rate of bone fragmentation, the density of lithic
818 debris/chips, the number of processed bones and their spatial density and association,
819 it is likely that the assemblage represents a complex palimpsest of locally repeated
820 events of hunting/scavenging and exploitation of lake shore resources. More data from
821 high resolution excavations in the coming years will allow us to refine the coarse-
822 grained spatio-temporal resolution of our inferences about past human behaviour at
823 Marathousa 1.

824 **5. Conclusions**

825 At the Middle Pleistocene open-air site of Marathousa 1, a partial skeleton of a
826 single individual of *Palaeoloxodon antiquus* was recovered in stratigraphic association
827 with a rich and consistent lithic assemblage and other vertebrate remains. Cut-marks
828 and percussion marks have been identified on the elephant and other mammal bones ex-
829 cavated at the site. The main find-bearing horizon represents a secondary depositional
830 process in a lake margin context.

831 Understanding the site formation processes is of primary importance in order to
832 reliably infer hominin exploitation of the elephant carcass and other animals. To meet
833 this aim, we applied a comprehensive set of multivariate and multiscale spatial analyses
834 in a taphonomic framework.

835 Results from the fabric, vertical distribution and point pattern analyses are consis-
836 tent with a high-energy erosional process, such as a hyperconcentrated flow deposited
837 at the margin of a swamp, reworking at a small scale an exposed (or slightly buried) and
838 consistent scatter of lithic artefacts and faunal remains. These results are in agreement
839 with preliminary taphonomic observations of the lithic artefacts ([Tourloukis et al., this issue](#)) and the faunal remains ([Konidaris et al., this issue](#)), which also indicate minor
840 weathering and transportation. Our analyses show that multiple lines of evidence sup-
841 port an autochthonous origin of the lithic and faunal assemblages, subject to minor
842 post-depositional reworking.
843

844 **Acknowledgements**

845 This research is supported by the European Research Council (ERC StG no. 283503
846 PaGE and ERC CoG no. 724703 CROSSROADS) awarded to K. Harvati. We are
847 grateful to the Municipality of Megalopolis, the authorities of the Region of Pelopon-
848 nese, and the Greek Public Power corporation (ΔΕΗ) for their support. We also thank
849 Julian Bega and all the participants in the PaGE survey and excavation campaigns in
850 Megalopolis for their indispensable cooperation. We are grateful to the editors and two
851 anonymous reviewers for their critical discussions and many constructive comments
852 that helped to improve this manuscript.

853 **References**

- 854 Anderson, K. L., Burke, A., 2008. Refining the definition of cultural levels at Karabi
855 Tamchin: a quantitative approach to vertical intra-site spatial analysis. *Journal of*
856 *Archaeological Science* 35 (8), 2274–2285.
- 857 Aramendi, J., Uribelarrea, D., Arriaza, M. C., Arráiz, H., Barboni, D., Yravedra, J.,
858 Ortega, M. C., Gidna, A., Mabulla, A., Baquedano, E., Domínguez-Rodrigo, M.,
859 2017. The paleoecology and taphonomy of AMK (Bed I, Olduvai Gorge) and its
860 contributions to the understanding of the “Zinj” paleolandscape. *Palaeogeography,*
861 *Palaeoclimatology, Palaeoecology* 488, 35–49.

- 862 Baddeley, A., Chang, Y.-M., Song, Y., Turner, R., 2012. Nonparametric estimation of
863 the dependence of a point process on spatial covariates. *Statistics and Its Interface*
864 5 (2), 221–236.
- 865 Bailey, G., 2007. Time perspectives, palimpsests and the archaeology of time. *Journal*
866 of Anthropological Archaeology 26 (2), 198–223.
- 867 Bar-Yosef, O., Tchernov, E., 1972. On the palaeo-ecological history of the site of Ubeidiya. Vol. 35. Israel Academy of Sciences and Humanities, Jerusalem.
- 869 Bargalló, A., Gabucio, M. J., Rivals, F., 2016. Puzzling out a palimpsest: Testing an
870 interdisciplinary study in level O of Abric Romaní. *Quaternary International* 417,
871 51–65.
- 872 Benito-Calvo, A., de la Torre, I., 2011. Analysis of orientation patterns in Olduvai
873 Bed I assemblages using GIS techniques: Implications for site formation processes.
874 *Journal of Human Evolution* 61 (1), 50–60.
- 875 Benito-Calvo, A., Martínez-Moreno, J., Mora, R., Roy, M., Roda, X., 2011. Trampling
876 experiments at Cova Gran de Santa Linya, Pre-Pyrenees, Spain: their relevance for
877 archaeological fabrics of the Upper–Middle Paleolithic assemblages. *Journal of Archaeological Science* 38 (12), 3652–3661.
- 879 Benito-Calvo, A., Martínez-Moreno, J., Pardo, J. F. J., de la Torre, I., Torcal, R. M.,
880 2009. Sedimentological and archaeological fabrics in Palaeolithic levels of the
881 South-Eastern Pyrenees: Cova Gran and Roca del Bous Sites (Lleida, Spain). *Journal*
882 of Archaeological Science 36 (11), 2566–2577.
- 883 Benn, D., 1994. Fabric shape and the interpretation of sedimentary fabric data. *Journal*
884 of Sedimentary Research 64 (4a), 910–915.
- 885 Benvenuti, M., Martini, I. P., 2002. Analysis of terrestrial hyperconcentrated flows and
886 their deposit. In: Martini, I. P., Baker, V. R., Garzón, G. (Eds.), *Flood and Megaflood*
887 *Processes and Deposits*. Vol. 32 of Special Publication of the International Association
888 of Sedimentologists. Blackwell Publishing Ltd., pp. 167–193.
- 889 Berman, M., 1986. Testing for spatial association between a point process and another
890 stochastic process. *Applied Statistics* 35, 54–62.
- 891 Bernatchez, J. A., 2010. Taphonomic implications of orientation of plotted finds from
892 Pinnacle Point 13B (Mossel Bay, Western Cape Province, South Africa). *Journal of*
893 *Human Evolution* 59 (3–4), 274–288.
- 894 Bertran, P., Hetù, B., Texier, J.-P., Steijn, H. V., 1997. Fabric characteristics of subaerial
895 slope deposits. *Sedimentology* 44 (1), 1–16.
- 896 Bertran, P., Texier, J.-P., 1995. Fabric Analysis: Application to Paleolithic Sites. *Journal*
897 of Archaeological Science 22 (4), 521–535.

- 898 Bevan, A., Crema, E., Li, X., Palmisano, A., 2013. Intensities, Interactions, and Un-
899 certainties: Some New Approaches to Archaeological Distributions. In: Bevan, A.,
900 Lake, M. (Eds.), Computational Approaches to Archaeological Spaces. Left Coast
901 Press, Walnut Creek, pp. 27–52.
- 902 Binford, L. R., 1981. Behavioral Archaeology and the "Pompeii Premise". *Journal of*
903 *Anthropological Research* 37 (3), 195–208.
- 904 Boschian, G., Saccà, D., 2010. Ambiguities in human and elephant interactions? Sto-
905 ries of bones, sand and water from Castel di Guido (Italy). *Quaternary International*
906 214 (1–2), 3–16.
- 907 Brantingham, P. J., Surovell, T. A., Waguespack, N. M., 2007. Modeling post-
908 depositional mixing of archaeological deposits. *Journal of Anthropological Archae-*
909 *ology* 26 (4), 517–540.
- 910 Carrer, F., 2015. Interpreting Intra-site Spatial Patterns in Seasonal Contexts: an Eth-
911 noarchaeological Case Study from the Western Alps. *Journal of Archaeological*
912 *Method and Theory*, 1–25.
- 913 Cobo-Sánchez, L., Aramendi, J., Domínguez-Rodrigo, M., 2014. Orientation patterns
914 of wildebeest bones on the lake Masek floodplain (Serengeti, Tanzania) and their
915 relevance to interpret anisotropy in the Olduvai lacustrine floodplain. *Quaternary*
916 *International* 322–323 (Supplement C), 277–284.
- 917 de la Torre, I., Benito-Calvo, A., 2013. Application of GIS methods to retrieve ori-
918 entation patterns from imagery; a case study from Beds I and II, Olduvai Gorge
919 (Tanzania). *Journal of Archaeological Science* 40 (5), 2446–2457.
- 920 Dibble, H. L., Chase, P. G., McPherron, S. P., Tuffreau, A., Oct. 1997. Testing the
921 reality of a "living floor" with archaeological data. *American Antiquity* 62 (4), 629–
922 651.
- 923 Diggle, P., 1985. A kernel method for smoothing point process data. *Applied Statistics*
924 (*Journal of the Royal Statistical Society, Series C*) 34, 138–147.
- 925 Domínguez-Rodrigo, M., Bunn, H., Mabulla, A., Baquedano, E., Uribelarrea, D.,
926 Pérez-González, A., Gidna, A., Yravedra, J., Diez-Martin, F., Egeland, C., Barba,
927 R., Arriaza, M., Organista, E., Ansón, M., 2014a. On meat eating and human evolu-
928 tion: A taphonomic analysis of BK4b (Upper Bed II, Olduvai Gorge, Tanzania), and
929 its bearing on hominin megafaunal consumption. *Quaternary International* 322–323,
930 129–152.
- 931 Domínguez-Rodrigo, M., Bunn, H., Pickering, T., Mabulla, A., Musiba, C., Baque-
932 dano, E., Ashley, G., Diez-Martin, F., Santonja, M., Uribelarrea, D., Barba, R.,
933 Yravedra, J., Barbón, D., Arriaza, C., Gidna, A., 2012. Autochthony and orientation
934 patterns in Olduvai Bed I: a re-examination of the status of post-depositional biasing
935 of archaeological assemblages from FLK North (FLKN). *Journal of Archaeological*
936 *Science* 39 (7), 2116–2127.

- 937 Domínguez-Rodrigo, M., Cobo-Sánchez, L., Yravedra, J., Uribelarrea, D., Arriaza, C.,
938 Organista, E., Baquedano, E., 2017. Fluvial spatial taphonomy: a new method for the
939 study of post-depositional processes. *Archaeological and Anthropological Sciences*.
- 940 Domínguez-Rodrigo, M., Diez-Martín, F., Yravedra, J., Barba, R., Mabulla, A., Baquedano,
941 E., Uribelarrea, D., Sánchez, P., Eren, M. I., 2014b. Study of the SHK Main
942 Site faunal assemblage, Olduvai Gorge, Tanzania: Implications for Bed II taphonomy,
943 paleoecology, and hominin utilization of megafauna. *Quaternary International*
944 322–323, 153–166.
- 945 Domínguez-Rodrigo, M., García-Pérez, A., 07 2013. Testing the Accuracy of Different
946 A-Axis Types for Measuring the Orientation of Bones in the Archaeological and
947 Paleontological Record. *PLoS ONE* 8 (7), e68955.
- 948 Domínguez-Rodrigo, M., Uribelarrea, D., Santonja, M., Bunn, H., García-Pérez, A.,
949 Pérez-González, A., Panera, J., Rubio-Jara, S., Mabulla, A., Baquedano, E., Yrave-
950 dra, J., Diez-Martín, F., 2014c. Autochthonous anisotropy of archaeological ma-
951 terials by the action of water: experimental and archaeological reassessment of the
952 orientation patterns at the Olduvai sites . *Journal of Archaeological Science* 41 (Sup-
953 plement C), 44–68.
- 954 Eberth, D. A., Rogers, R. R., Fiorillo, A. R., 2007. A practical approach to the study of
955 bonebeds. In: Rogers, R. R., Eberth, D. A., Fiorillo, A. R. (Eds.), *Bonebeds. Genesis,*
956 *Analysis, and Paleobiological Significance*. The University of Chicago Press, pp.
957 265–332.
- 958 Enloe, J. G., 2006. Geological processes and site structure: assessing integrity at a Late
959 Paleolithic open-air site in northern France. *Geoarchaeology* 21 (6), 523–540.
- 960 Eren, M. I., Durant, A., Neudorf, C., Haslam, M., Shipton, C., Bora, J., Korisettar,
961 R., Petraglia, M., 2010. Experimental examination of animal trampling effects on
962 artifact movement in dry and water saturated substrates: a test case from South India.
963 *Journal of Archaeological Science* 37 (12), 3010–3021.
- 964 Fernández-López, S. R., 1991. Taphonomic concepts for a theoretical biochronology.
965 *Revista Española de Paleontología* 6, 37–49.
- 966 Fiorillo, A. R., 1991. Taphonomy and depositional setting of Careless Creek Quarry
967 (Judith River Formation), Wheatland County, Montana, U.S.A. *Palaeogeography,*
968 *Palaeoclimatology, Palaeoecology* 81 (3), 281–311.
- 969 Frison, G. C., Todd, L. C., 1986. *The Colby Mammoth Site: Taphonomy and Archae-
970 ology of a Clovis Kill in Northern Wyoming*. University of New Mexico Press.
- 971 García-Moreno, A., Smith, G. M., Kindler, L., Pop, E., Roebroeks, W., Gaudzinski-
972 Windheuser, S., Klinkenberg, V., 2016. Evaluating the incidence of hydrological
973 processes during site formation through orientation analysis. A case study of the
974 middle Palaeolithic Lakeland site of Neumark-Nord 2 (Germany). *Journal of Ar-
975 chaeological Science: Reports* 6, 82–93.

- 976 Giusti, D., Arzarello, M., 2016. The need for a taphonomic perspective in spatial analy-
977 sis: Formation processes at the Early Pleistocene site of Pirro Nord (P13), Apricena,
978 Italy. *Journal of Archaeological Science: Reports* 8, 235–249.
- 979 Harvati, K., Panagopoulou, E., Tourloukis, V., Thompson, N., Karkanas, P., Athanasi-
980 siou, A., Konidaris, G., Tsartsidou, G., Giusti, D., 2016. New Middle Pleistocene
981 elephant butchering site from Greece. In: Paleoanthropology Society Meeting. At-
982 lanta, Georgia, pp. A14–A15.
- 983 Hivernel, F., Hodder, I., 1984. Analysis of artifact distribution at Ngenym (Kenya):
984 depositional and postdepositional effects. In: Hietala, H., Larson, P. (Eds.), *Intrasite*
985 *Spatial Analysis in Archaeology*. Cambridge University Press, Ch. 7, pp. 97–115.
- 986 Hodder, I., Orton, C., 1976. *Spatial Analysis in Archaeology. New Studies in Archae-*
987 *ology*. Cambridge University Press, Cambridge.
- 988 Hovers, E., Ekshtain, R., Greenbaum, N., Malinsky-Buller, A., Nir, N., Yeshurun, R.,
989 2014. Islands in a stream? Reconstructing site formation processes in the late Middle
990 Paleolithic site of 'Ein Qashish, northern Israel. *Quaternary International* 331, 216–
991 233.
- 992 Isaac, G. L., 1967. Towards the interpretation of occupation debris: Some experiments
993 and observations. *Kroeber Anthropological Society Papers* 37 (37), 31–57.
- 994 Jammalamadaka, S., Sengupta, A., Sengupta, A., 2001. *Topics in Circular Statistics.*
995 Series on multivariate analysis. World Scientific.
- 996 Karkanas, P., Tourloukis, V., Thompson, N., Giusti, D., Panagopoulou, E., Harvati, K.,
997 this issue. Sedimentology and micromorphology of the Lower Palaeolithic lakeshore
998 site Marathousa 1, Megalopolis basin, Greece. *Quaternary International*.
- 999 Kluskens, S. L., 1990. Orientation and density analysis of stone artefacts at Combe-
1000 Capelle Bas, Périgord, France. Master's thesis, University of Pennsylvania.
- 1001 Konidaris, G., Athanassiou, A., Tourloukis, V., Thompson, N., Giusti, D.,
1002 Panagopoulou, E., Harvati, K., this issue. The skeleton of a straight-tusked elephant
1003 (*Palaeoloxodon antiquus*) and other large mammals from the Middle Pleistocene
1004 butchering locality Marathousa 1 (Megalopolis Basin, Greece): preliminary results.
1005 *Quaternary International*.
- 1006 Krumbein, W. C., 1941. Measurement and geological significance of shape and round-
1007 ness of sedimentary particles. *Journal of Sedimentary Research* 11 (2), 64–72.
- 1008 Kuiper, 1960. Tests concerning random points on a circle. *Proceedings of the Konin-*
1009 *klijke Nederlandse Akademie van Wetenschappen, Series A* 63, 38—47.
- 1010 Lenoble, A., Bertran, P., 2004. Fabric of Palaeolithic levels: methods and implications
1011 for site formation processes. *Journal of Archaeological Science* 31 (4), 457–469.

- 1012 Lenoble, A., Bertran, P., Lacrampe, F., 2008. Solifluction-induced modifications
 1013 of archaeological levels: simulation based on experimental data from a modern
 1014 periglacial slope and application to French Palaeolithic sites. *Journal of Archaeo-*
 1015 *logical Science* 35 (1), 99–110.
- 1016 Lindsay, J. F., 1968. The development of clast fabric in mudflows. *Journal of Sedimen-*
 1017 *tary Research* 38 (4), 1242–1253.
- 1018 Macdonald, D. I. M., Jefferson, T. H., 1985. Orientation studies of waterlogged wood;
 1019 a paleocurrent indicator? *Journal of Sedimentary Research* 55 (2), 235–239.
- 1020 Malinsky-Buller, A., Hovers, E., Marder, O., 2011. Making time: ‘Living floors’,
 1021 ‘palimpsests’ and site formation processes – A perspective from the open-air Lower
 1022 Paleolithic site of Revadim Quarry, Israel. *Journal of Anthropological Archaeology*
 1023 30 (2), 89–101.
- 1024 Marwick, B., 2017. Computational reproducibility in archaeological research: Ba-
 1025 sic principles and a case study of their implementation. *Journal of Archaeological*
 1026 *Method and Theory* 24 (2), 424–450.
- 1027 Marwick, B., d’Alpoim Guedes, J., Barton, C. M., Bates, L. A., Baxter, M., Beavan,
 1028 A., Bollwerk, E. A., Bocinsky, R. K., Brughams, T., Carter, A. K., Conrad, C.,
 1029 Contreras, D. A., Costa, S., Crema, E. R., Daggett, A., Davies, B., Drake, B. L.,
 1030 Dye, T. S., France, P., Fullager, R., Giusti, D., Graham, S., Harris, M. D., Hawks, J.,
 1031 Heath, S., Huffer, D., Kansa, E. C., Kansa, S. W., Madsen, M. E., Melcher, J., Negre,
 1032 J., Neiman, F. D., Opitz, R., Orton, D. C., Przystupa, P., Raviele, M., Riel-Salvatore,
 1033 J., Riris, P., Romanowska, I., Smith, J., Strupler, N., Ullah, I. I., Vlack, H. G. V.,
 1034 VanValkenberg, N., Watrall, E. C., Webster, C., Wells, J., Winters, J., Wren, C. D.,
 1035 2017. Open science in archaeology. *SAA Archaeological Record* 17 (4), 8–14.
- 1036 McPherron, S. J., 2005. Artifact orientations and site formation processes from total
 1037 station proveniences. *Journal of Archaeological Science* 32 (7), 1003–1014.
- 1038 McPherron, S. J., Dibble, H. L., Goldberg, P., 2005. Z. *Geoarchaeology* 20 (3), 243–
 1039 262.
- 1040 Morton, A. G. T., 2004. Archaeological Site Formation: Understanding Lake Margin
 1041 Contexts. Vol. 1211 of International Series. British Archaeological Reports, Oxford.
- 1042 Nickel, B., Riegel, W., Schonherr, T., Velitzelos, E., 1996. Environments of coal forma-
 1043 tion in the Pleistocene lignite at Megalopolis, Peloponnese (Greece) - reconstruc-
 1044 tion from palynological and petrological investigations. *N. Jb. Geol. Palaont. A.* 200,
 1045 201–220.
- 1046 Ohser, J., 1983. On estimators for the reduced second moment measure of point pro-
 1047 cesses. *Mathematische Operationsforschung und Statistik, series Statistics* 14, 63–
 1048 71.

- 1049 Organista, E., Domínguez-Rodrigo, M., Yravedra, J., Uribelarrea, D., Arriaza, M. C.,
 1050 Ortega, M. C., Mabulla, A., Gidna, A., Baquedano, E., 2017. Biotic and abiotic pro-
 1051 cesses affecting the formation of BK Level 4c (Bed II, Olduvai Gorge) and their bear-
 1052 ing on hominin behavior at the site. *Palaeogeography, Palaeoclimatology, Palaeo-
 1053 ecology* 488, 59–75.
- 1054 Orton, C., 1982. Stochastic process and archaeological mechanism in spatial analysis.
 1055 *Journal of Archaeological Science* 9 (1), 1–23.
- 1056 Panagopoulou, E., Tourloukis, V., Thompson, N., Athanassiou, A., Tsartsidou, G.,
 1057 Konidaris, G., Giusti, D., Karkanas, P., Harvati, K., 2015. Marathousa 1: a new Mid-
 1058 dle Pleistocene archaeological site from Greece. *Antiquity Project Gallery* 89 (343).
- 1059 Petraglia, M. D., Nash, D. T., 1987. The impact of fluvial processes on experimen-
 1060 tal sites. In: Nash, D. T., Petraglia, M. D. (Eds.), *Natural formation processes and*
 1061 *the archaeological record*. Vol. 352 of International Series. British Archaeological
 1062 Reports, Oxford, pp. 108–130.
- 1063 Petraglia, M. D., Potts, R., 1994. Water Flow and the Formation of Early Pleistocene
 1064 Artifact Sites in Olduvai Gorge, Tanzania . *Journal of Anthropological Archaeology*
 1065 13 (3), 228–254.
- 1066 Pewsey, A., Neuhauser, M., Ruxton, G. D., 2013. Circular Statistics in R. Oxford
 1067 University Press.
 1068 URL [http://www.ebook.de/de/product/21010817/arthur_pewsey_](http://www.ebook.de/de/product/21010817/arthur_pewsey_markus_neuhauser_graeme_d_ruxton_circular_statistics_in_r.html)
 1069 [markus_neuhauser_graeme_d_ruxton_circular_statistics_in_r.html](http://www.ebook.de/de/product/21010817/arthur_pewsey_markus_neuhauser_graeme_d_ruxton_circular_statistics_in_r.html)
- 1070 Pierson, T. C., 2005. Distinguishing between debris flows and floods from field evi-
 1071 dence in small watersheds. USGS Numbered Series, U.S. Geological Survey.
- 1072 R Core Team, 2017. R: A Language and Environment for Statistical Computing. R
 1073 Foundation for Statistical Computing, Vienna, Austria.
 1074 URL <https://www.R-project.org/>
- 1075 Ripley, B., 1977. Modelling spatial patterns. *Journal of the Royal Statistical Society,*
 1076 *series B* 39, 172–212.
- 1077 Ripley, B., 1988. Statistical inference for spatial processes. Cambridge University
 1078 Press.
- 1079 Ripley, B. D., 1976. The second-order analysis of stationary point processes. *Journal*
 1080 *of Applied Probability* 13 (2), 255–266.
- 1081 Ripley, B. D., 1981. Spatial Statistics. John Wiley and Sons, New York.
- 1082 Schick, K. D., 1984. Processes of paleolithic site formation: an experimental study.
 1083 Ph.D. thesis, University of California, Berkeley.
- 1084 Schick, K. D., 1986. Stone Age sites in the making: experiments in the formation
 1085 and transformation of archaeological occurrences. Vol. 319 of International Series.
 1086 British Archaeological Reports, Oxford.

- 1087 Schick, K. D., 1987. Modeling the formation of Early Stone Age artifact concentrations. *Journal of Human Evolution* 16, 789–807.
- 1088
- 1089 Schiffer, M. B., 1972. Archaeological Context and Systemic Context. *American Antiquity* 37 (2), 156–165.
- 1090
- 1091 Schiffer, M. B., 1983. Toward the identification of formation processes. *American Antiquity* 48 (4), 675–706.
- 1092
- 1093 Schiffer, M. B., 1987. Formation processes of the archaeological record. University of New Mexico Press, Albuquerque.
- 1094
- 1095 Shackley, M. L., 1978. The behaviour of artefacts as sedimentary particles in a fluvial environment. *Archaeometry* 20 (1), 55–61.
- 1096
- 1097 Sánchez-Romero, L., Benito-Calvo, A., Pérez-González, A., Santonja, M., 12 2016. Assessment of Accumulation Processes at the Middle Pleistocene Site of Ambrona (Soria, Spain). Density and Orientation Patterns in Spatial Datasets Derived from Excavations Conducted from the 1960s to the Present. *PLOS ONE* 11 (12), 1–27.
- 1098
- 1099
- 1100
- 1101 Texier, J.-P., 2000. A propos des processus de formation des sites préhistoriques / About prehistoric site formation processes. *Paléo* 12 (1), 379–386.
- 1102
- 1103 Toots, H., 1965. Orientation and distribution of fossils as environmental indicators. In: Nineteenth Field Conference of the Wyoming Geological Association. pp. 219–292.
- 1104
- 1105 Tourloukis, V., Thompson, N., Panagopoulou, E., Giusti, D., Konidaris, G., Karkanas, P., Harvati, K., this issue. Lithic artifacts and bone tools from the Lower Palaeolithic site of Marathousa 1, Megalopolis, Greece: preliminary results. *Quaternary International*.
- 1106
- 1107
- 1108
- 1109 van Vugt, N., de Bruijn, H., van Kolfschoten, M., Langereis, C. G., 2000. Magneto- and cyclostratigraphy and mammal-fauna's of the Pleistocene lacustrine Megalopolis Basin, Peloponnesos, Greece. *Geologica Ultrajectina* 189, 69–92.
- 1110
- 1111
- 1112 Vaquero, M., Chacón, M. G., García-Antón, M. D., de Soler, B. G., Martínez, K., Cuartero, F., 2012. Time and space in the formation of lithic assemblages: The example of Abric Romaní Level J. *Quaternary International* 247 (0), 162–181.
- 1113
- 1114
- 1115 Villa, P., 2004. Taphonomy and stratigraphy in european prehistory. *Before Farming* 2004 (1), 1–20.
- 1116
- 1117 Voorhies, M., 1969. Taphonomy and population dynamics of an early Pliocene vertebrate fauna, Knox County, Nebraska. *Contributions to Geology, University of Wyoming Special Paper* 1, 1–69.
- 1118
- 1119
- 1120 Walter, M. J., Trauth, M. H., 2013. A MATLAB based orientation analysis of Acheulean handaxe accumulations in Olorgesailie and Kariandusi, Kenya Rift. *Journal of Human Evolution* 64 (6), 569–581.
- 1121
- 1122
- 1123 Watson, 1961. Goodness-of-fit tests on a circle. *Biometrika* 48 (1/2), 109–114.

- 1124 Wood, R. W., Johnson, D. L., 1978. A survey of disturbance processes in archaeological
1125 site formation. In: Schiffer, M. B. (Ed.), Advances in archaeological method and
1126 theory. Vol. 1. Academic Press, Ch. 9, pp. 315–381.
- 1127 Woodcock, N., Naylor, M., 1983. Randomness testing in three-dimensional orientation
1128 data. Journal of Structural Geology 5 (5), 539–548.